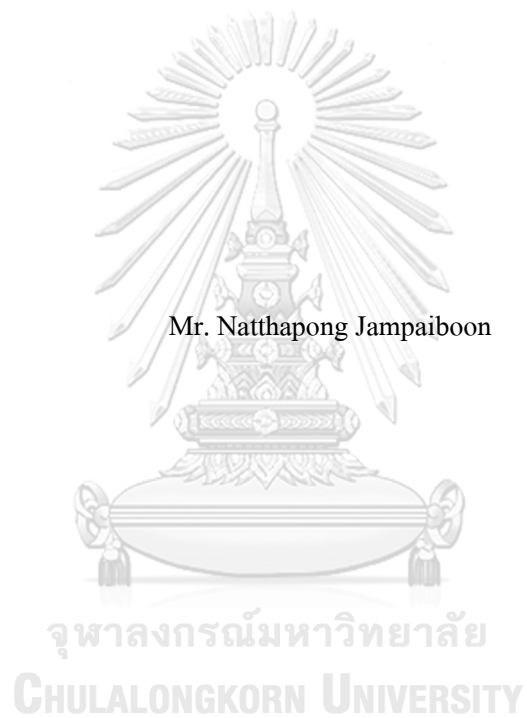


MULTIPOLE RESONANCE PROBE MEASUREMENT IN PLASMA



A Thesis Submitted in Partial Fulfillment of the Requirements

for the Degree of Master of Science in Physics

Department of Physics

FACULTY OF SCIENCE

Chulalongkorn University

Academic Year 2019

Copyright of Chulalongkorn University

การวัดด้วยหัววัดแบบเส้นพ้องหลายขั้วในพลาสมา



วิทยานิพนธ์นี้เป็นส่วนหนึ่งของการศึกษาตามหลักสูตรปริญญาวิทยาศาสตรมหาบัณฑิต
สาขาวิชาฟิสิกส์ ภาควิชาฟิสิกส์
คณะวิทยาศาสตร์ จุฬาลงกรณ์มหาวิทยาลัย
ปีการศึกษา 2562
ลิขสิทธิ์ของจุฬาลงกรณ์มหาวิทยาลัย

Thesis Title	MULTIPOLE RESONANCE PROBE MEASUREMENT IN PLASMA
By	Mr. Natthapong Jampaiboon
Field of Study	Physics
Thesis Advisor	Associate Professor BOONCHOAT PAOSAWATYANYONG, Ph.D.

Accepted by the FACULTY OF SCIENCE, Chulalongkorn University in Partial
Fulfillment of the Requirement for the Master of Science

..... Dean of the FACULTY OF SCIENCE
(Professor POLKIT SANGVANICH, Ph.D.)

THESIS COMMITTEE

..... Chairman
(Assistant Professor PATCHA CHATRAPORN, Ph.D.)

..... Thesis Advisor
(Associate Professor BOONCHOAT PAOSAWATYANYONG,
Ph.D.)

..... Examiner
(Assistant Professor NORAVEE KANCHANAVATEE, Ph.D.)

..... External Examiner
(Associate Professor Thawatchai Onjun)

ณัฐพงษ์ แจ่มไพบูลย์ : การวัดด้วยหัววัดแบบสั้นพ้องหลายขั้วในพลาสมา. (MULTIPOLE RESONANCE PROBE MEASUREMENT IN PLASMA) อ.ที่ปรึกษา
หลัก : รศ. ดร.บุญโชติ เผ่าสวัสดิ์ชัยรยง

หัววัดแบบสั้นพ้องเป็นหนึ่งในวิธีที่ใช้ศึกษาพลาสมา วิธีนี้สามารถหลีกเลี่ยงปัญหาการปนเปื้อนในระบบที่เกิดขึ้นจากหัววัดเชิงไฟฟ้าแบบลางค์มัวได้ เนื่องจากลักษณะของหัววัดที่ถูกหุ้มด้วยวัสดุไดอิเล็กตริก ทำให้หัววัดไม่สัมผัสกับพลาสมาโดยตรง หัววัดแบบสั้นพ้อง มีได้หลายรูปทรง เช่น หัววัดแบบครึ่งทรงกลม แบบก้นหอย หรือรูปทรงอิสระ เป็นต้น หัววัดเชิงไฟฟ้าแบบสั้นพ้องหลายขั้ว เป็นหัววัดที่มีรูปร่างเป็นครึ่งทรงกลมและได้รับความสนใจในการศึกษา ทั้งนี้เพราะทรงกลมเป็นรูปทรงที่สามารถหาผลเฉลยทางคณิตศาสตร์ของศักย์ไฟฟ้าได้ง่ายที่สุดจากการแก้สมการลาปลาซในพิกัดทรงกลมแบบมีสมมาตร ในการศึกษาหัววัดแบบครึ่งทรงกลม แบบแผ่นบางคู่ และแบบเสาคู่ขนาน ได้ถูกสร้างขึ้น เพื่อใช้ในการวัดค่าความหนาแน่นพลาสมาโดยการเชื่อมต่อหัววัดกับอุปกรณ์วิเคราะห์ความถี่เพื่อหาความถี่แม่ทซ์จากสัมประสิทธิ์การสะท้อน แล้วจึงสอบเทียบความถี่แม่ทซ์กับค่าความหนาแน่นพลาสมาที่ได้จากหัววัดเชิงไฟฟ้าแบบลางค์มัว ผลการทดลองจากการสอบเทียบได้ถูกเปรียบเทียบกับผลการทดลองที่ได้จากโมเดลคณิตศาสตร์ของหัววัดเชิงไฟฟ้าแบบครึ่งทรงกลม ผลการศึกษาพบว่า ค่าความหนาแน่นของพลาสมาที่ได้จากโมเดลทางคณิตศาสตร์จะให้ค่าความหนาแน่นพลาสมามากกว่าวิธีการสอบเทียบหัววัดโดยใช้หัววัดเชิงไฟฟ้าแบบลางค์มัวประมาณ 100 เท่า

จุฬาลงกรณ์มหาวิทยาลัย
CHULALONGKORN UNIVERSITY

สาขาวิชา ฟิสิกส์
ปีการศึกษา 2562

ลายมือชื่อนิติ
ลายมือชื่อ อ.ที่ปรึกษาหลัก

6171950623 : MAJOR PHYSICS

KEYWORD: Active plasma resonance spectroscopy, Multipole resonance probe

Natthapong Jampaiboon : MULTIPOLE RESONANCE PROBE MEASUREMENT
IN PLASMA. Advisor: Assoc. Prof. BOONCHOAT PAOSAWATYANYONG,
Ph.D.

Active plasma resonance spectroscopy (APRS) is one of the interesting methods which could avoid plasma contamination problem occurs in a conventional Langmuir probe measurement. It is because the probe conductors are covered by a dielectric material. The APRS probe can be of any shape. A multipole resonance probe is a hemisphere APRS probe since a sphere imposes the simplest way to find an analytical solution by solving the Laplace equation in the spherical coordinates with the azimuthal symmetry. In this study, the APRS probes in the hemisphere, microstrip, and parallel rod shapes were constructed. Plasma density was obtained by using the probe that is connected with a network analyzer to locate the match frequencies in the reflection coefficient spectrum. The match frequencies of different probe shapes were then calibrated with the plasma density obtained by Langmuir probe measurement. Our experiments showed that the constructed probes respond with the change in plasma. For the hemisphere probe, the results of the calibrated and the mathematically analyzed results were compared. Our study showed that the plasma density from the mathematical model is approximately the second order of magnitude away from that of the Langmuir probe.

Field of Study: Physics

Student's Signature

Academic Year: 2019

Advisor's Signature

ACKNOWLEDGEMENTS

I would like to express my sincere gratitude to my thesis adviser Dr. Boonchoat Paosawatyanong for his support, academic knowledge, and work techniques. I also would like to thank my committee members, Dr. Patcha Chatraporn, Dr. Noravee Kanjanavatee, and Dr. Thawatchai Onjun for their valuable comments and knowledge.

Many thanks go to Mr. Chatchai Sirithipvanich who spent many hours helping me throughout this research. I also would like to thank Sahaporntool limited partnership for all technical support and fabrication of the probes used in our experiments.

My greatest appreciation goes out to my parent, and friends, their encouragement give me the strength to finish the work. A special thanks to Kanyaphat for her love, support, and patience over a few years.

I thank the Department of physics, Chulalongkorn University for support throughout this research. In addition, I thank the Science Achievement Scholarship of Thailand (SAST) for scholarships.

Natthapong Jampaiboon

TABLE OF CONTENTS

	Page
ABSTRACT (THAI).....	iii
ABSTRACT (ENGLISH).....	iv
ACKNOWLEDGEMENTS.....	v
TABLE OF CONTENTS.....	vi
LIST OF FIGURES.....	1
LIST OF TABLES.....	5
1. INTRODUCTION.....	6
2. PLASMA CHARACTERISTICS AND PARAMETER ANALYSIS.....	13
2.1 CHAPTER OVERVIEW.....	13
2.2 QUASI-NEUTRALITY.....	13
2.3 COLLECTIVE BEHAVIOR.....	16
2.4 STATISTICAL MODEL FOR LOW-TEMPERATURE PLASMA.....	16
2.5 MAXWELL VELOCITY DISTRIBUTION.....	17
2.6 BOLTZMANN RELATION.....	18
2.7 PLASMA SHEATH.....	18
2.8 SHEATH EQUATION.....	19
2.9 PRESHEATH.....	20
2.10 ELECTRICAL PROBE.....	21
2.11 DC PLASMA DISCHARGE.....	23
3. DC PLASMA SYSTEM AND ELECTRICAL PROBE MEASUREMENT.....	24
3.1 CHAPTER OVERVIEW.....	24

3.2 PLASMA CHAMBER.....	24
3.3 VACUUM SYSTEM	25
3.4 ELECTRIC SYSTEM.....	26
3.5 THE CONSTRUCTED LANGMUIR PROBE.....	28
3.6 LANGMUIR PROBE MEASUREMENT	30
4. ACTIVE PLASMA RESONANCE SPECTROSCOPY	32
4.1 CHAPTER OVERVIEW	32
4.2 TRANSMISSION LINE THEORY	32
4.3 LOSSLESS TRANSMISSION LINE	35
4.4 TRANSMISSION LINE RESONATOR	37
5. HEMISPHERE PROBE.....	40
5.1 CHAPTER OVERVIEW	40
5.2 HEMISPHERE PROBE SOLUTION.....	40
5.3 HEMISPHERE PROBE DISSIPATED POWER SIMULATION	45
6. PROBE CONSTRUCTION AND MEASUREMENT SYSTEM.....	49
6.1 CHAPTER OVERVIEW	49
6.2 HEMISPHERE PROBE.....	49
6.3 MICROSTRIP PROBE	50
6.4 PARALLEL PROBE.....	50
6.5 MEASUREMENT SYSTEM.....	51
7. PROBE MEASUREMENTS	54
7.1 CHAPTER OVERVIEW	54
7.1 HEMISPHERE PROBE MEASUREMENT	54
7.2 MICROSTRIP PROBE MEASUREMENT.....	59

7.3 PARALLEL PROBE MEASUREMENT	62
8. PROBE CALIBRATIONS	65
8.1 CHAPTER OVERVIEW	65
8.2 HEMISPHERE PROBE CALIBRATION	65
8.3 MICROSTRIP PROBE CALIBRATION	67
8.4 PARALLEL PROBE CALIBRATION	69
8.4 LANGMUIR PROBE PLASMA DENSITY AND MATCH FREQUENCY RELATION	71
9. DISCUSSION	73
10. SUMMARY	75
APPENDIX A	76
DEBYE LENGTH.....	76
PLASMA FREQUENCY.....	77
MAXWELL VELOCITY DISTRIBUTION	78
BOLTZMANN RELATION.....	79
SHEATH EQUATION	80
APPENDIX B	81
REFERENCES	83
VITA	86

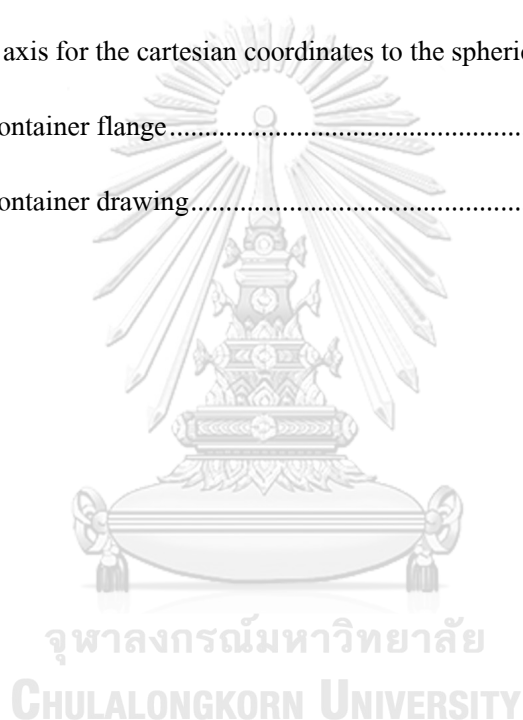
LIST OF FIGURES

Figure 1 Schematic diagram of the microwave resonator probe [4].....	7
Figure 2 (a) Schematic of the excitation of plasma oscillation by beam injection and (b) potential profile near the filament [3]	8
Figure 3 Plasma absorption probe schematic [5]	8
Figure 4 Schematics of hairpin probes (a) dc-coupled and (b) fully floating [8]	9
Figure 5 Multipole resonance probe schematic [7].....	9
Figure 6 The prototype of the multipole resonance probe [9]	10
Figure 7 Abstract model for N-electrode system [6]	10
Figure 8 Planar multipole resonance probe schematic [2].....	11
Figure 9 Semi-neutral state of the plasma that is disturbed by positive and negative charges	14
Figure 10 The potential of the plasma (Φ) at various distances compared with the potential from disturbance charges (Φ_0).....	14
Figure 11 Maxwell velocity distribution in 1 dimension	17
Figure 12 The electric potential within the sheath and the pre-sheath when the plasma interacts with the wall.....	18
Figure 13 (a) Circuit diagram for measuring the voltage-current of a single probe (b) Typical I-V characteristic for a Langmuir probe	21
Figure 14 The clearly divided regions of the plasma in low-pressure systems	23
Figure 15 Vacuum chamber schematic	24
Figure 16 Vacuum chamber	25
Figure 17 Vacuum system diagram.....	25
Figure 18 Vacuum equipment.....	26
Figure 19 Electric system of DC plasma diagram	26

Figure 20 Air plasma at 0.13 mbar	27
Figure 21 Argon plasma at 0.25 mbar.....	27
Figure 22 Schematics diagram of Langmuir probe.....	28
Figure 23 Langmuir probe prototype with BNC conductor.....	28
Figure 24 Langmuir probe measurement system.....	28
Figure 25 Langmuir probe Equipment.....	29
Figure 26 The I-V characteristic example at power 2.055 watts that obtained from DC plasma by using the constructed Langmuir probe at any DC generated power	30
Figure 27 The plasma densities are obtained from the DC plasma by using the constructed Langmuir probe at any DC generated power.....	30
Figure 28 Lumped-element equivalent circuit of a transmission line section	33
Figure 29 A lossless transmission line terminated by a Z_L impedance load	35
Figure 30 A transmission line with a finite length l with Z_L as a single load	37
Figure 31 Schematic diagram of the hemisphere probe.....	40
Figure 32 The hemisphere probe regions.....	41
Figure 33 Flowchart for determining the simulation of dissipated power	46
Figure 34 The simulation of the electrostatic potential at (r, θ) around the hemisphere probe ...	47
Figure 35 The simulation of the electric field at (r, θ) around the hemisphere probe.....	48
Figure 36 The simulation of the dissipated power at Legendre polynomial order 1 to 17	48
Figure 37 Schematics of hemisphere probe	49
Figure 38 (a) 16 millimeters microstrip and (b) 21 millimeters microstrip	50
Figure 39 (a) 16 millimeters parallel, and (b) 21 millimeters parallel.....	50
Figure 40 E5071C ENA Vector Network Analyzer	51
Figure 41 The type of connector	52

Figure 42 The probes measurement system	52
Figure 43 Hemisphere probe and Langmuir probe were measured simultaneously at the same location.....	53
Figure 44 The system of plasma density measurement	53
Figure 45 The reflection coefficients were obtained from the DC plasma by using the constructed hemisphere probe at any DC generated power	54
Figure 46 The match frequencies were obtained from the DC plasma by using the constructed hemisphere probe at any DC generated power	55
Figure 47 The plasma densities are obtained from the DC plasma by using the constructed hemisphere probe at any DC generated power	55
Figure 48 Comparison of the plasma density obtained from the constructed hemisphere probe and the constructed Langmuir probe.....	57
Figure 49 The reflection coefficient of the 16 mm. microstrip at any DC generated power	59
Figure 50 The reflection coefficient of the 21 mm. microstrip at any DC generated power	59
Figure 51 The plasma densities are obtained from the DC plasma by using the microstrip at any electric power	61
Figure 52 The reflection coefficient of the 16 mm. parallel at any DC generated power	62
Figure 53 The reflection coefficient of the 21 mm. parallel at any DC generated power	62
Figure 54 The match frequencies are obtained from the DC plasma by using the microstrip at any DC generated power	64
Figure 55 The relation of plasma density obtained from Langmuir probe	66
Figure 56 The relation of the average plasma density obtained from the Langmuir probe.....	67
Figure 57 The relation of the average plasma density obtained from the Langmuir probe.....	68
Figure 58 The relation of the average plasma density obtained from the Langmuir probe.....	69

Figure 59 The relation of the average plasma density obtained from Langmuir probe and the average 21 mm. parallel match frequency square.....	70
Figure 60 The relation between the average Langmuir probe plasma density and the match frequency of active resonance probe in each shape	71
Figure 61 The relation between the average Langmuir probe plasma density and the average match frequency square of active resonance probe in each shape	72
Figure 62 The occurrence of an electric field when the electron particles move in 2D[1].....	77
Figure 63 Reference axis for the cartesian coordinates to the spherical coordinates in 3D [1].....	78
Figure 64 Vacuum container flange.....	81
Figure 65 Vacuum container drawing.....	82



LIST OF TABLES

Table 1 Summary table of plasma densities from DC plasma measurement by using Langmuir probe.....	31
Table 2 The constants of various variables	47
Table 3 Summary table of match frequency, and plasma densities from DC plasma measurement by using hemisphere probe	56
Table 4 Summary table of plasma densities from DC plasma measurement by using Langmuir and hemisphere probe	57
Table 5 Summary table of the match frequency of 16 mm., and 21 mm. microstrip.....	60
Table 6 Summary table of the match frequency of 16 mm., and 21 mm. parallel.....	63
Table 7 Summary table of plasma density from DC plasma measurement by using a Langmuir probe and hemisphere match frequency.....	66
Table 8 Summary table of plasma density from DC plasma measurement by using a Langmuir probe and Microstrip match frequency	68
Table 9 Summary table of plasma density from DC plasma measurement by using a Langmuir probe and Microstrip match frequency	70
Table 10 Summary table of the average plasma density from DC plasma measurement by using a Langmuir probe and the average match frequency of any probe shape.....	71
Table 11 Summary table of the average plasma density from DC plasma measurement by using a Langmuir probe and the average match frequency of any probe shape.....	72

1. INTRODUCTION

Low-temperature plasma has been used in industries, such as the synthesis of thin-film, plasma treatments, and surface-property modification. In the study of low-temperature plasma, the plasma parameters such as plasma density and plasma temperature are required [10]. One of the most popular methods for measuring plasma parameters is the Langmuir probe measurement [11]. The advantages of the probe are localized and simple measurement set up. Additionally, the probe can detect various parameters including plasma temperature, plasma density, plasma potential, and plasma-floating potential. However, the probe must be inserted directly into the plasma which leads to disadvantages in unavoidable plasma perturbation and the probe contamination due to the sputtered metal molecules from the tip [12].

Active plasma resonance spectroscopy (APRS) is another area of plasma diagnostic technique [6]. It is the terminology for the probes which are composed of dielectric materials and conductors. The probes can be of any shape such as hemisphere, planar, spiral, microstrip, and parallel. Plasma absorption probe, multipole resonance probe, planar multipole resonance probe, and curling probe are among the well-known APRS probe [5, 7, 13-16]. The probe tip of the APRS probe will not directly contact the plasma. Therefore, it does not cause contamination due to the sputtered metal molecules from the tip [6]. When the probes are inserted into plasma, we consider the probe and plasma as a system of electrical networks. The system's reflection coefficients over a range of frequencies are measured and analyzed into the plasma density.

The origin of the APRS probe was introduced from the idea of a transmission line resonator. The first probe is a microwave resonator. The microwave resonator characteristic is a parallel-wire quarter-wavelength resonator as shown in Figure 1. The probe was invented by Stenzel, R. L. et al. in 1976 to determine the plasma density as equation (1) and the cold plasma dielectric properties as equation (2) via the resonance frequency based on the microwave technique [4].

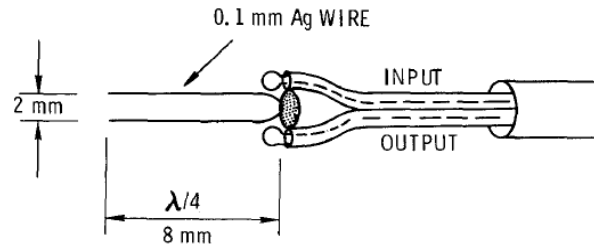


Figure 1 Schematic diagram of the microwave resonator probe [4]

$$n_e = \varepsilon_0 m_e \omega_{pe}^2 / e^2 \quad (1)$$

$$\varepsilon = 1 - \frac{\omega_{pe}^2}{\omega^2} \quad (2)$$

In their work, a parallel-wire resonator was inserted into a uniform medium of dielectric constant ε . Propagation constant is

$$k = (\omega/c)\varepsilon^{1/2} \quad (3)$$

A quarter-wavelength ($kl = \pi/2$) exhibits a resonance at

$$\omega_{res} = \left(\frac{\pi}{2l}\right) \left(\frac{c}{\varepsilon^{1/2}}\right) \quad (4)$$

Resonance frequency in vacuum (vacuum dielectric constant = 1) exhibits at

$$\omega_{res(\varepsilon=1)} = \frac{\pi c}{2l} \quad (5)$$

According to equation (3), (4), and (5), plasma frequency becomes the equation (6) [4] and plasma density can be collected from equation (1).

$$\omega_{pe}^2 = \omega_{res}^2 - \omega_{res(\varepsilon=1)}^2 \quad (6)$$

where ω_{pe} is the plasma frequency

In 1993, Shirakawa, T. et al. proposed the plasma oscillation method to determine the plasma density. A weak electron beam was injected to excite electron wave oscillation as shown in Figure 2. The detector was connected with a spectrum analysis to obtain the plasma frequency. Finally, the plasma density can be obtained from equation (1). The plasma densities results are in good agreement with a Langmuir probe [3].

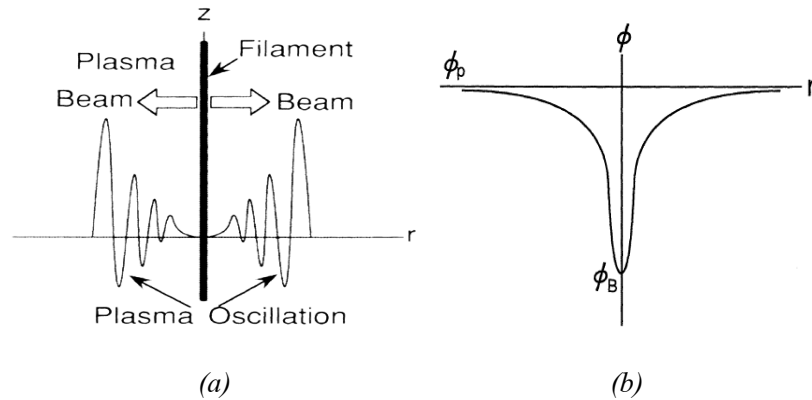


Figure 2 (a) Schematic of the excitation of plasma oscillation by beam injection and (b) potential profile near the filament [3]

In 1999, the plasma absorption probe (PAP) was invented by Kokura, H. et al. The probe consists of a small antenna enclosed in a dielectric tube of dielectric constant ϵ , as shown in Figure 3. The probes analysis was based on the resonance absorption of surface waves excited in a cavity at the probe head. The surface wave resonance frequency (ω_{SW}) is shown in equation (7). The probe was connected with a network analyzer. This was the first APRS probe that used a network analyzer to obtain the reflection coefficient. The reflection coefficient spectrum was first utilized to determine the plasma frequency and the plasma density can be obtained from equation (1) [5].

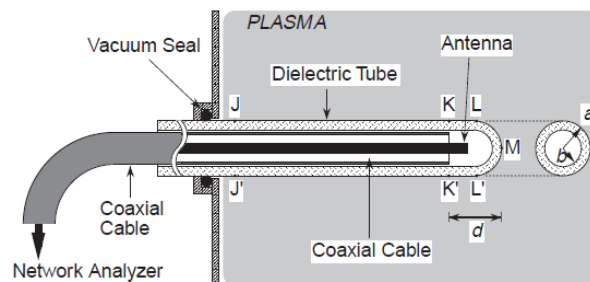


Figure 3 Plasma absorption probe schematic [5]

$$\omega_{SW} = \omega_p / (1 + \epsilon)^{1/2} \quad (7)$$

In 2004, Piejak, R.B. et al. developed a hairpin resonator probe from a microwave resonator and modified to increase coupling to the hairpin structure. In addition, it also minimized plasma perturbations and enabled a greater range of plasma density measurements. The probe was used reflection mode rather than transmission mode [8]. The hairpin probe has 2 types which are a dc-coupled hairpin and a fully floating hairpin as shown in Figure 4.

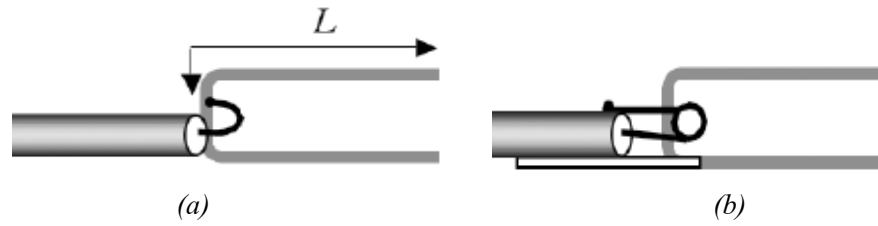


Figure 4 Schematics of hairpin probes (a) dc-coupled and (b) fully floating[8]

In 2007, Lapke, M. et al. proposed the first analytical model for the determination of the voltage reflection coefficient spectrum experiments and simulations of plasma absorption probe measurements [13]. Lapke, M. et al. proposed a new solution derived from plasma surface wave propagating along with an infinite dielectric cylinder. The calculations are in good qualitative agreement with the surface wave proposed by Kokura, H et al. The probe characteristics are the same as the plasma absorption probe by Kokura, H [5].

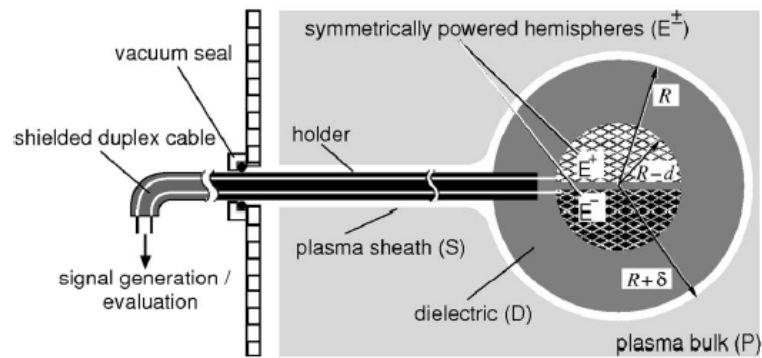


Figure 5 Multipole resonance probe schematic [7]

In 2008, the two-hemisphere multipole resonance probe (MRP) concept was also presented by Lapke, M. et al. Multipole resonance probe schematic is shown in Figure 5. The probe was a model for analytically determining the relation between the dissipated power spectrum and the electrostatic potential as equation (8). The solution of the multipole resonance probe electrostatic potential was derived based on cold plasma conditions. The electrostatic potential can be obtained by solving the Laplace equation in the spherical coordinate with azimuthal symmetry [7].

$$S(\omega) = \int_p \frac{\epsilon_0 v \omega_{pe}^2}{2(v^2 + \omega^2)} |\nabla \Phi|^2 d^3 r \quad (8)$$

In 2011, The prototype of the multipole resonance probe was constructed by Lapke, M. et al. as shown in Figure 6. The probe size is 10 mm. in diameter. The experimental results are conformed with both the analytic model proposed in 2008 and the Langmuir probe measurements in RF plasma generator [9].

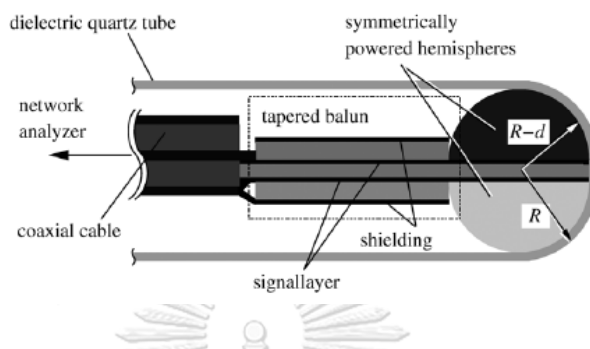


Figure 6 The prototype of the multipole resonance probe[9]

In 2014, the active plasma resonance spectroscopy (APRS) was proposed by Oberrath J. et al. in 2014. The mathematical model of an arbitrarily shaped probe was written in a compact equation. The matrix representation of the resolvent of the dynamical operator was determined. The eigenvalues of the matrix represented the resonance frequency and electron density [17].

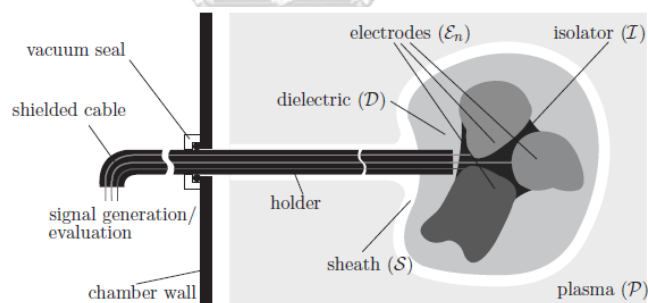


Figure 7 Abstract model for N-electrode system[6]

Recently, the planar multipole resonance probe (pMRP) was proposed by Schulz C. et al. in 2015. The analytic method was improved by Friedrich, M. in 2018. The probe was design based on the multipole resonance probe [2, 14]. The hemisphere multipole resonance probe was reduced to a single half-disc which can be integrated into the chamber wall as shown in Figure 8.

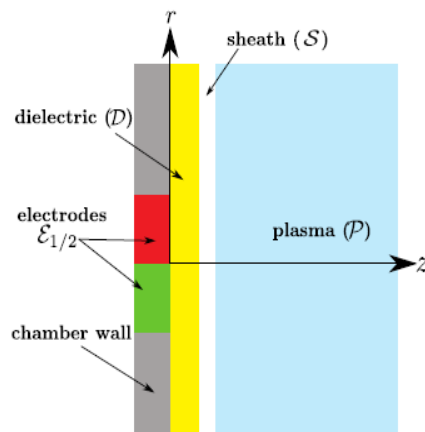


Figure 8 Planar multipole resonance probe schematic[2]

One of the interesting APRS probes was the multipole resonance probe proposed by Martin Lapke in 2008 [7]. The probe characteristic is a simple design consisting of two hemispheres conductor, insulated and covered by a thin dielectric sheath. The name of the multipole resonance probe comes from an analytical solution of electrostatic potential using multipole expansion.

The solution of the multipole resonance probe is the one possible way to find the mathematical model by solving the Laplace equation in the spherical coordinate. Multipole resonance probe is an interesting probe because the advantages of the probe are simple and localized measurement similar to that of the Langmuir probe but do not cause plasma contamination. However, the probe can only measure plasma density. Presently, the multipole resonance probe is not widely applicable and only investigated by a single group of researchers.

In this study, the plasma parameter measurements of the different probe tip shapes including hemisphere, microstrip, and parallel will be constructed to measure the plasma density of the probes in DC plasma. The simplest way is to calibrate against the conventional Langmuir probe plasma density. The system's reflection coefficients over a range of frequencies are measured and analyzed into the plasma density. Presently, the hemisphere probe shape is the only one that has an analytical solution. The solution of the hemisphere probe was used to determine the plasma density. The results are verified against those of the Langmuir probe in order to confirm that the hemisphere probe can actually be utilized to determine the plasma density. If the probe worked as it was claimed, the techniques would be a good candidate for other well-established and robust method of plasma diagnostics.

This thesis is divided into 10 chapters. After an introduction in this current first chapter, the thesis is organized and covered in the following order. Chapter 2 provides a background on plasma characteristics, parameter analysis, previous studies of conventional Langmuir probe, and DC plasma discharge. Chapter 3 presents the details of DC plasma system, Langmuir probe construction, Langmuir probe measurement, and equipment used in this research. Chapter 4 describes active plasma resonance spectroscopy and the transmission line resonator based on the transmission line theory. Chapter 5 exhibits the solution of active plasma resonance spectroscopy in hemisphere shape and the dissipated power simulation. Chapter 6 shows the probe construction including the active plasma resonance spectroscopy probe in the hemisphere, microstrip line, and parallel rod. Chapter 7 shows the results of active plasma resonance spectroscopy probe measurement and the effect of pressure on the hemisphere probe. Chapter 8 elaborates the calibration methods to find the plasma density of any probe shapes from the experiment match frequency. Chapter 9 presents a discussion of this research and suggestions for future work. Finally, chapter 10 presents the analysis of the results and conclusion of the study.

2. PLASMA CHARACTERISTICS AND PARAMETER ANALYSIS

2.1 CHAPTER OVERVIEW

This chapter presents the detail of plasma characteristics and the basic method for determining the plasma parameter. Plasma occurs by changes in atoms in the gas state when receiving enough energy, atoms are ionized and transformed into particles consist of positive charged ions and electrons which are negatively charged. To determine whether the group of interested particles is plasma or not. It must consist of 2 properties which are quasi-neutrality, and collective behavior [1]. The next section will discuss a statistical model for low-temperature plasma. In thermal equilibrium, the particles have all value of the velocities. The most probability distribution of velocities is known as Maxwell velocity distribution and the electron density at various locations can be described by the Boltzmann relation. Next, the details of the plasma sheath which is the basis of parameter analysis using the electrical probe are described. The traditional measurement method of the electrical probe which is the Langmuir probe is elaborated. The probe is used to measure the plasma density in a DC plasma discharge. Finally, the detail on DC plasma discharge is shown in the last section of this chapter.

2.2 QUASI-NEUTRALITY

As already stated above, the plasma exhibits the quasi-neutrality which means that the total net charge is approximately zero [1]. It can be seen as a neutral state. But when the plasma is considered in a small area, it is not neutral. Therefore, it can be estimated that within the plasma, electrons and ions have a similar charge density.

$$n_i \approx n_e \quad (9)$$

where n_i is the ion density in the plasma

n_e is the electron density in the plasma

The behavior of the plasma always keeps the total charge at about zero, therefore, plasma has the ability to prevent increased electric potential due to charge or external interference. This property allows the plasma to return to a semi-neutral state as in Figure 9, the plasma can maintain the neutral state from the disturbance charge entering the plasma area.

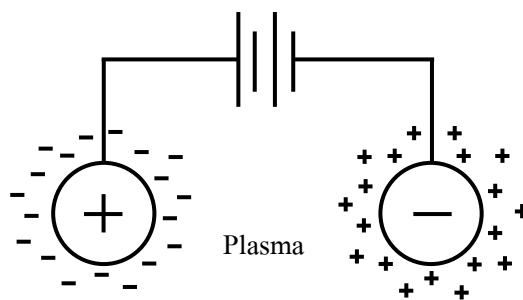


Figure 9 Semi-neutral state of the plasma that is disturbed by positive and negative charges

Debye length is a value that indicates the area of disturbed charge entering the plasma [1]. When the distance from the disturbing charge exceeds the Debye length. It is estimated that the difference between the electric potential due to the disturbing charge and the electric potential in the plasma is near zero. This means that at a distance greater than the Debye length, the disturbing charge will not affect the plasma as shown in Figure 10. More details of the Debye length are given in Appendix A.

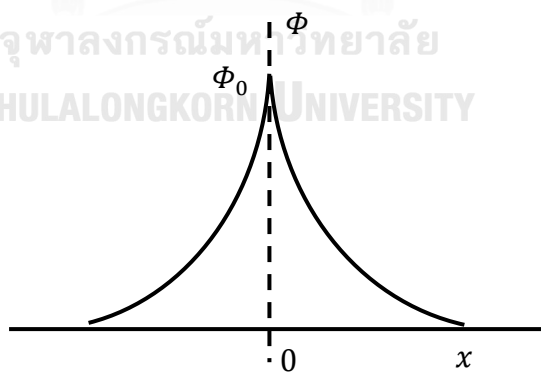


Figure 10 The potential of the plasma (Φ) at various distances compared with the potential from disturbance charges (Φ_0)

Debye length can be calculated from the equation [1]

$$\lambda_D = \sqrt{\frac{kT_e \epsilon_0}{ne^2}} \quad (10)$$

where λ_D is Debye length

k is Boltzmann constant which is equal to $1.3806 \times 10^{-23} \text{ JK}^{-1}$

T_e is electron temperature (K)

ϵ_0 is vacuum permittivity which is equal to $8.8542 \times 10^{-12} \text{ Fm}^{-1}$

n is electron density (n_e) or ion density (n_i) in plasma

e is electron charge which is equal to $1.6022 \times 10^{-19} \text{ C}$

From the quasi-neutrality property, it can be said that the plasma is different from the gas. Plasma is a gas that has been ionized. Plasma consists of particles that have both positive and negative charges. But it does not mean that all the gases that have been ionized are plasma. The number of internal particles can be considered from the number of particles within the spherical sphere [11] which can be calculated as the equation (10) where N_D is the number of particles within the Debye sphere

$$N_D = n \frac{4}{3} \pi \lambda_D^3 \quad (11)$$

From equation (11), it can be seen that if the Debye sphere is small, the number of particles in the Debye sphere will also be less. Therefore, it can be concluded that the number of particles within the spherical sphere must not be too small. Another requirement is the total number of particles in the Debye sphere must be much greater than one particle because if the Debye sphere contains only a few particles, it will be impossible to estimate the plasma by using statistical principles.

$$N_D \gg 1 \quad (12)$$

2.3 COLLECTIVE BEHAVIOR

Not only that the plasma must be quasi-neutrality as mention in the previous section, plasma also must have special properties, namely collective behavior. Negative and positive charges have electrical interactions. Plasma group behavior indicates that the particles in the plasma must oscillate [11]. Therefore, the particles will have both vibrations and motions at the same time. The movement will cause particle collisions. Collision will cause the plasma to return to a normal gas state. The detail of plasma frequency is given in Appendix A

$$\omega_{pe} = \sqrt{\frac{ne^2}{\epsilon_0 m}} \quad (13)$$

where ω_{pe} is plasma frequency

m is a mass charge

If there are many collisions in the plasma. Plasma would lose energy due to the collisions which may cause a lack of plasma properties. Therefore, special conditions for any particles are not to collide too much as shown in the equation (14). The plasma frequency must be greater than the frequency of particle collisions

$$\omega_p > \nu_m \quad (14)$$

where ν_m is the average frequency of collisions in the plasma particles

2.4 STATISTICAL MODEL FOR LOW-TEMPERATURE PLASMA

In order to describe the low-temperature plasma that observes quasi-neutrality, and collective behavior, we use a statistical model. The assumptions in the plasma statistical model consist of [11]

1. The electrons inside the plasma are in a thermal equilibrium state.
2. The mass of a positive charge is approximately 3600 times higher than the mass of electrons. In low-temperature plasma, it can be estimated that electrons move at a speed much faster than the speed of positive charges. Therefore, it can be considered that the positive charges standstill as compared to the electrons.

2.5 MAXWELL VELOCITY DISTRIBUTION

As the previous section, which is a statistical model, the model that is commonly used to describe the velocities of electrons is Maxwell velocities distribution. In low-temperature plasma, the electrons behave under the thermal equilibrium at various speeds under the Maxwell distribution [1]. The detail of Maxwell velocity distribution is included in Appendix A

$$f(\vec{v}) = n_e \left(\frac{m_e}{2\pi kT} \right)^{\frac{3}{2}} \exp\left(-\frac{m_e v^2}{2kT}\right) \quad (15)$$

where $f(\vec{v})$ is the electron velocity distribution function
 \vec{v} is the electron velocity
 v is the electron speed
 m_e is the electron mass
 n_e is the electron density
 T is the system temperature

Example of Maxwell speed distribution with a single velocity in 1 dimension (where v is the speed in 1 dimension)

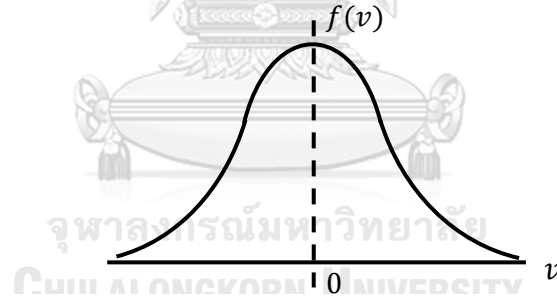


Figure 11 Maxwell velocity distribution in 1 dimension

The velocity distribution of this electron can be used to calculate the average electron speed and the electron flux in one dimension. When the electrons are in thermal equilibrium, the average electron speed is found to be

$$\langle v \rangle = \sqrt{\frac{2kT_e}{\pi m_e}} \quad (16)$$

where $\langle v \rangle$ is the average electron speed

$$\Gamma = \frac{1}{4} n_e \langle v \rangle \quad (17)$$

where Γ is the electron flux in one dimension. The detail of average electron speed and electron flux in one dimension is given in Appendix A.

2.6 BOLTZMANN RELATION

When the electrons are in the thermal equilibrium, the Boltzmann relation is used to describe the electron density in various locations. It can be written as [1]

$$n_e(\vec{r}) = n_0 \exp\left(\frac{e\Phi(\vec{r})}{kT_e}\right) \quad (18)$$

where $\Phi(\vec{r})$ is the electrical potential

n_0 is the electron density without electric field

e is the electron charge

More detail on Boltzmann relation is given in Appendix A

2.7 PLASMA SHEATH

In general, plasma is equipotential since there is no field in the plasma. If there is a wall or any device that has another potential coming into the plasma, it will create a voltage difference between the two areas which is called a plasma sheath [11]. Plasma sheath is divided into 2 regions which are sheath and presheath as in Figure 12. The potential that changes within the sheath can be calculated from the equation of the sheath without collisions.

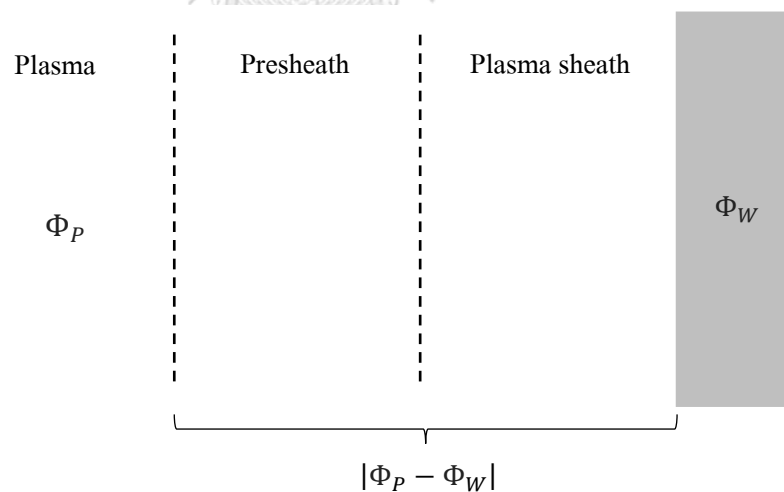


Figure 12 The electric potential within the sheath and the pre-sheath when the plasma interacts with the wall

2.8 SHEATH EQUATION

In order to describe the plasma sheath, the sheath equation can be realized by using the conservation of energy of ion without collisions together with the continuity equation by using electron density from the Boltzmann relations [11]. The sheath equation can be written in equation (19.1). The detail of the sheath equation is given in Appendix A

$$\frac{d^2 \Phi(x)}{dx^2} = \frac{en_s}{\epsilon_0} \left[\exp\left(\frac{e\Phi(x)}{kT_e}\right) - \left(1 - \frac{\Phi(x)}{\mathcal{E}_s}\right)^{\frac{1}{2}} \right] \quad (19.1)$$

$$e\mathcal{E}_s = \frac{1}{2}Mu_s^2 \quad (19.2)$$

where Φ is sheath potential

n_s is the density of charged particles at the plasma edge of the sheath

$e\mathcal{E}_s$ is the energy of the positive charge before entering the sheet

M is a mass of positive charge

u_s is the speed of the positive charge before entering the sheath

When multiplying the equation (19.1) with $\frac{d\Phi}{dx}$ and finding the integral with the variable x , we can obtain

$$\frac{1}{2} \left(\frac{d\Phi}{dx}\right)^2 = \frac{en_s}{\epsilon_0} \left[\frac{kT_e}{e} \exp\left(\frac{e\Phi}{kT_e}\right) - \frac{kT_e}{e} + 2\mathcal{E}_s \left(1 - \frac{\Phi}{\mathcal{E}_s}\right)^{\frac{1}{2}} - 2\mathcal{E}_s \right] \quad (20)$$

Given that $\Phi = 0$ and $\frac{d\Phi}{dx} = 0$ at $x = 0$, when considering the area of the sheath that is next to the plasma. Φ is small compared to kT_e and $2\mathcal{E}_s$, the equation (20) can be estimated by using the second-ranks Taylor series [11].

$$\frac{1}{2} \left(\frac{d\Phi}{dx}\right)^2 = \frac{en_s}{\epsilon_0} \left[\frac{1}{2} \frac{e\Phi^2}{kT_e} - \frac{\Phi^2}{4\mathcal{E}_s} \right] \quad (21)$$

It can be clearly seen that the right-hand side of the equation (21) needs to be greater than zero. Since the left side of the equation is the power of the first derivative that can be written as an inequality equation as

$$\frac{1}{2} \Phi^2 \left[\frac{e}{kT_e} - \frac{1}{2\mathcal{E}_s} \right] \geq 0 \quad (22.1)$$

$$\mathcal{E}_s \geq \frac{1}{2} \frac{kT_e}{e} \quad (22.2)$$

Substitute the value in (119.2) to get

$$u_s \geq u_B = \left(\frac{kT_e}{M} \right)^{\frac{1}{2}} \quad (23)$$

The equation (23) can be interpreted as the speed of positive charges before entering the sheath. It must be at least equal to Bohm's speed (u_B) which is known as Bohm's Criteria for plasma sheath.

2.9 PRESHEATH

From the velocity of the positive charge before entering the plasma sheath as shown in the previous section, the speed must be at least equal to Bohm's speed. The velocity of the positive charges within the plasma is always less than the threshold for the Bohm's criteria. Therefore, there must be an area between the plasma and the plasma sheath which is responsible for accelerating the positive charge. In order to get enough energy to cross the boundary to enter the sheath area. Consider the potential area before the sheath, it can accelerate the positive charge to be a speed greater than Bohm's criteria [11]

$$\frac{1}{2} M u_B^2 = e \Phi_P \quad (24)$$

where Φ_P is the potential difference between the edges before the plasma sheath

When substituting u_B from equation (23) in equation (24), we get

$$\Phi_P = \frac{1}{2} \frac{kT_e}{e} \quad (25)$$

From the Boltzmann relation (18), it is possible to calculate the density of positive and negative charged particles at the boundary of the sheath and the pre-sheath.

$$n_s = n \exp\left(-\frac{e\Phi_P}{kT_e}\right) \approx 0.61n \quad (26)$$

where n_s, n is the density of positive or negative charge particles at the boundary of the pre-sheath at the sheath side and the plasma side respectively.

2.10 ELECTRICAL PROBE

In order to study the plasma parameters, one of the most important electrical probes is the Langmuir probe. The probe was introduced by Mott-Smith and Langmuir in 1926 [11, 12]. the probe must be inserted directly into the plasma to obtain electron or ion current. The definition of voltage and current are defined in Figure 13 (a) which lead to a typical probe voltage-current characteristic or I-V characteristic as shown in Figure 13 (b) [11, 12]

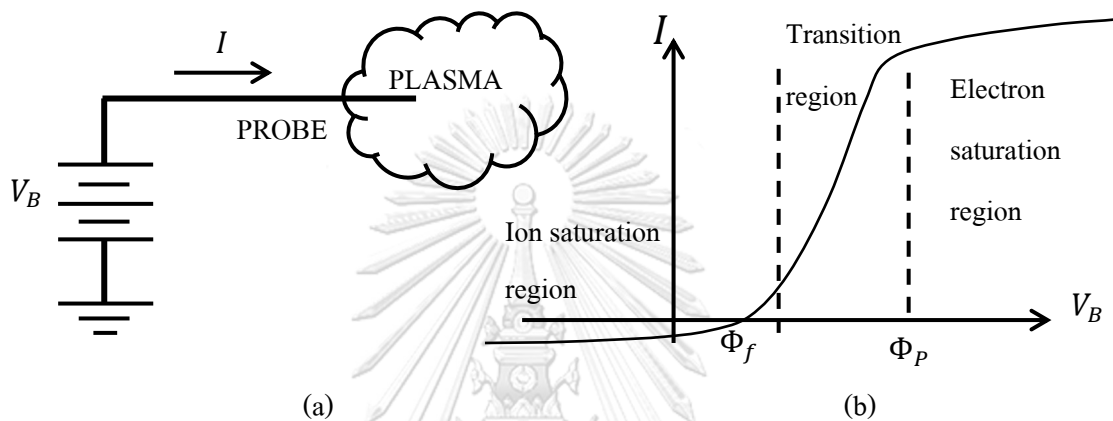


Figure 13 (a) Circuit diagram for measuring the voltage-current of a single probe

(b) Typical I-V characteristic for a Langmuir probe

The current which flows into the probe is considered from Kirchoff's Current Law.

$$I = -I_i + I_e \quad (27)$$

where I is the current flowing into the probe system

I_i is the current that the probe system loses to plasma due to positive charges

I_e is the current that the probe system receives from the plasma due to electrons

According to Bohm's criteria (equation 23), the density of positive charge particles (equation 26), and the current density of positive charges. Therefore, the current equation of positive charges flowing into the probe is [11]

$$I_i = 0.61neA\sqrt{\frac{kT_e}{M}} \quad (28)$$

where A is the surface area of the probe that contact with the plasma

While the current of electrons flowing into the probe, the electron flux in one dimension (Γ) from equation (17) combined with the Boltzmann relation from equation (18) that describes the electron density. When there is a potential difference [11]

$$I_e = \frac{1}{4} ne \langle v \rangle A \exp \frac{e(V - \Phi_P)}{kT_e} \quad (29)$$

where V is the potential difference between the probe and the ground

Φ_P is the potential difference between the plasma and the ground

The equation (29) works well when the potential difference between the probe and the plasma is less than zero. When the potential difference between the probe and the plasma is greater than zero, the electron current will be saturated [11]

$$I_e = I_{esat} = e\Gamma A = \frac{1}{4} ne \langle v \rangle A \quad (30)$$

where I_{esat} is the saturated electron current

Γ is the electron flux in one dimension

The combination of the equation (28), (29), and (30) will be a graph of the I-V characteristic for a Langmuir probe as shown in Figure 13(b). Applying logarithm to the equation (30) [11]

$$\ln I_e = \ln I_{esat} + \frac{e(V - \Phi_P)}{kT_e} \quad (31)$$

The derivative of $\ln I_e$ with respect to V

$$\frac{d \ln I_e}{dV} = \frac{e}{kT_e} \quad (32)$$

We can calculate the electron temperature from equation (32) and substitute the electron temperature into equation (28). The density of charged particles in the plasma can be collected. For the analysis of plasma parameters from the I-V characteristic, the measured current in the equation (27) is the total current. It can be clearly divided into 3 areas which are the current area due to saturated positive charges, transition area, and the current area due to saturated electrons as in Figure 13 (b). Therefore, calculating the derivatives in (32), it is necessary to deduct the current due to the positive charge first. The deduction of the current due to the positive charge causing current errors. Therefore, the area that can be used to calculate the electron temperature is only the transition area.

2.11 DC PLASMA DISCHARGE

In the study of the plasma parameter, the plasma system used is DC plasma of argon plasma. DC plasma can be created by using two electrodes which are anode and cathode. Electrons are accelerated to move from the cathode to the anode. When the electrons move, it will collide with an atom, and ions or the collisions of electrons. During the collision, electrons transfer energy to the particle. For collisions between electrons and atoms, if the collision has enough energy transfer, the electrons in atoms are stimulated to go up to the excited state. As the electron falls back from the excited state to the ground state, the energy is released as light. Allowing us to see plasma with various lights according to the type of inserting gas. The DC plasma in a vacuum container glows which can be observed clearly in low-pressure plasma systems. The closest part to the ideal plasma is the bright side of the anode (positive column), which is used in the study [18].

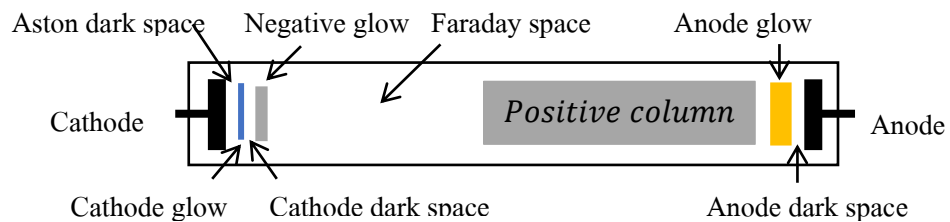


Figure 14 The clearly divided regions of the plasma in low-pressure systems

3. DC PLASMA SYSTEM AND ELECTRICAL PROBE MEASUREMENT

3.1 CHAPTER OVERVIEW

This chapter presents the details of the DC plasma discharge system and the Langmuir probe measurement. The plasma system used for the study of plasma parameters is the DC plasma of argon gas. It starts by describing the characteristics and the components of the plasma chamber. The plasma chamber was vacuumed by connecting to a vacuum pump and provided voltage by using the DC power supply. This chapter also gives details on equipment and experimental setup. The Langmuir probe was used to measure the plasma density in DC plasma. The details on probe characteristics and experiment setup are shown in the last two sections of this chapter.

3.2 PLASMA CHAMBER

To achieve low pressure, the system must be pressure controlled. The container consists of 2 flanges of stainless steel, gas and probe delivery ports, air pump connector, and the pressure gauge connector. The vacuum chamber body is made of borosilicate glass, diameter 80 millimeters, length 20 centimeters. Inside, there are electrodes which are made of brass. The negative and positive electrode has a channel in the middle of the stainless-steel plate so that the multipole resonance probe and Langmuir probe can be inserted into the system. There are O-rings every connector point to control the vacuum in the container. The vacuum chamber schematics and vacuum chamber used in this experiment are shown in Figure 15 and Figure 16.

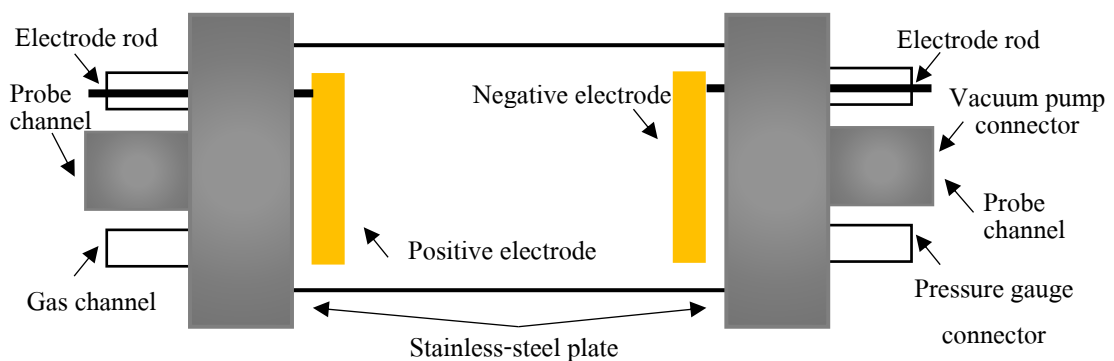


Figure 15 Vacuum chamber schematic

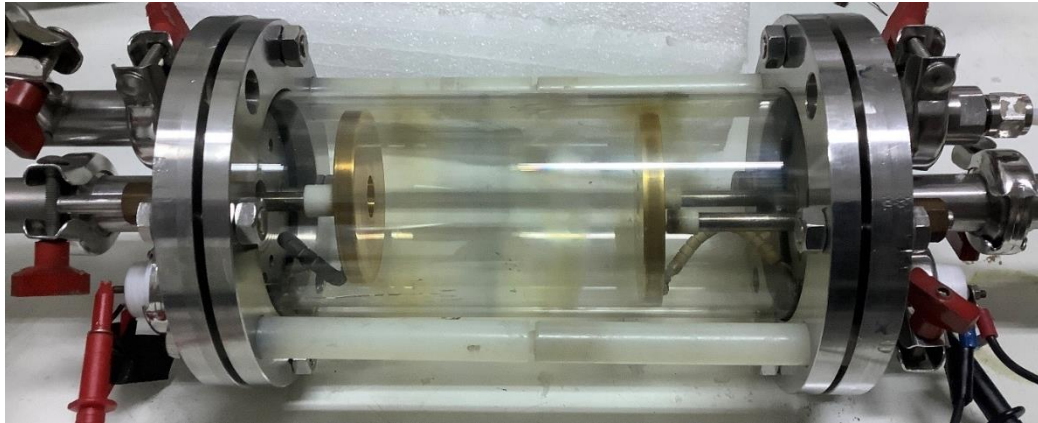


Figure 16 Vacuum chamber

3.3 VACUUM SYSTEM

The vacuum chamber was pumped out all the time by the vacuum pump GVD-3 produced by Atlas Copco which can read the minimum pressure of 10^{-3} millibar vacuum. The Edward API-100 active Pirani gauge which can read an absolute pressure gauge range between 10^{-4} - 10^3 millibar used to read the pressure. To manipulate pressure, connectors were connected with a diaphragm Speedivalves produced by Edwards. The Aalborg GFC17 argon mass flow controller was used to regulate argon gas flow to the chamber. The vacuum system diagram and the picture of the vacuum pump, diaphragm valve, pressure gauge, and mass flow controller are shown in Figure 17 and Figure 18.

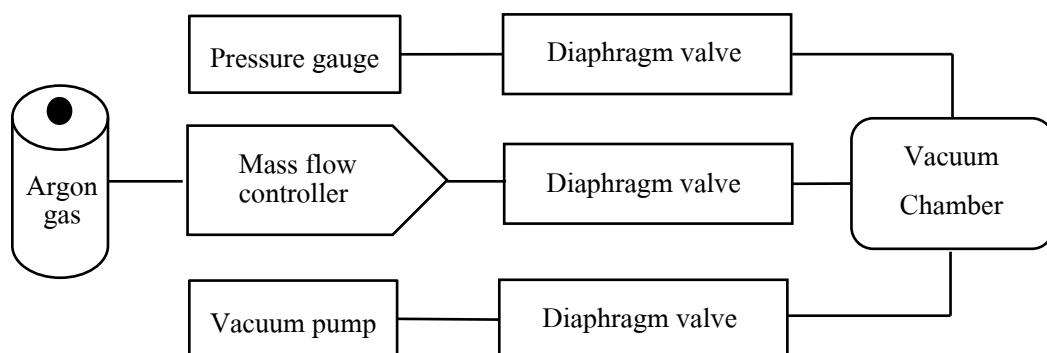


Figure 17 Vacuum system diagram



3.4 ELECTRIC SYSTEM

Creating plasma from DC, the potential difference between the two electrodes must be high to be enough to ionize the plasma. The equipment used to provide voltage is a GPR-60H15D DC power supply produced by GW Instek which can supply up to 900 watts of power as shown in Figure 18 (e). The device connects with size resistance $10\text{ k}\Omega$ to prevent short circuits which may damage the DC power supply device. The electric system of DC plasma is shown in Figure 19.

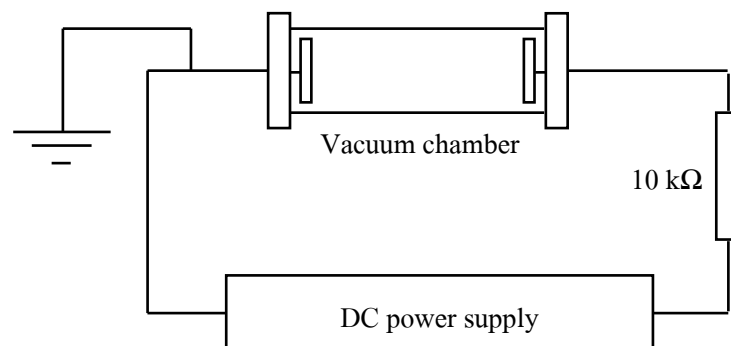


Figure 19 Electric system of DC plasma diagram

In the process of generating a plasma from argon gas. The plasma was created by using a DC system. The result of air plasma and argon plasma was shown in Figures 20 and 21.

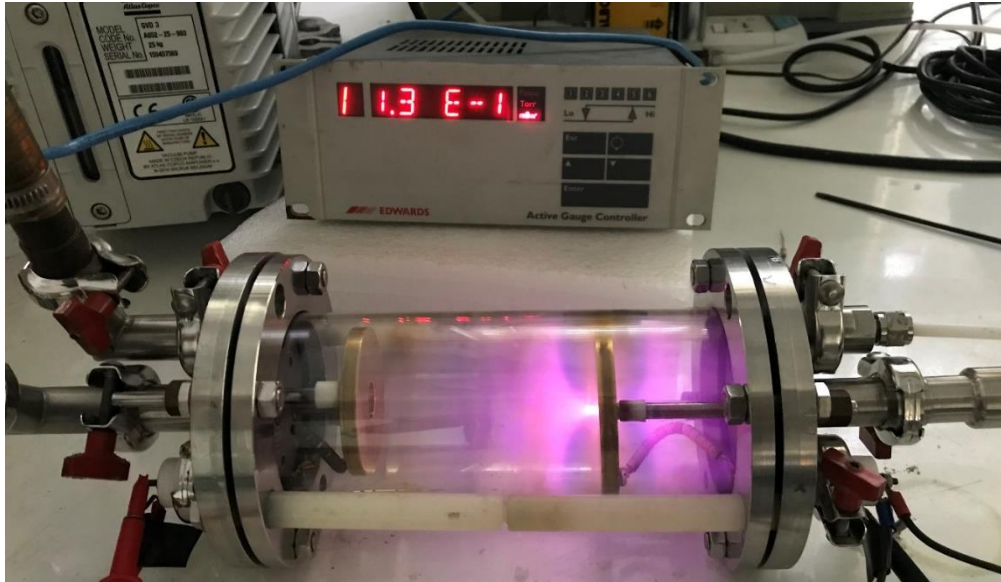


Figure 20 Air plasma at 0.13 mbar

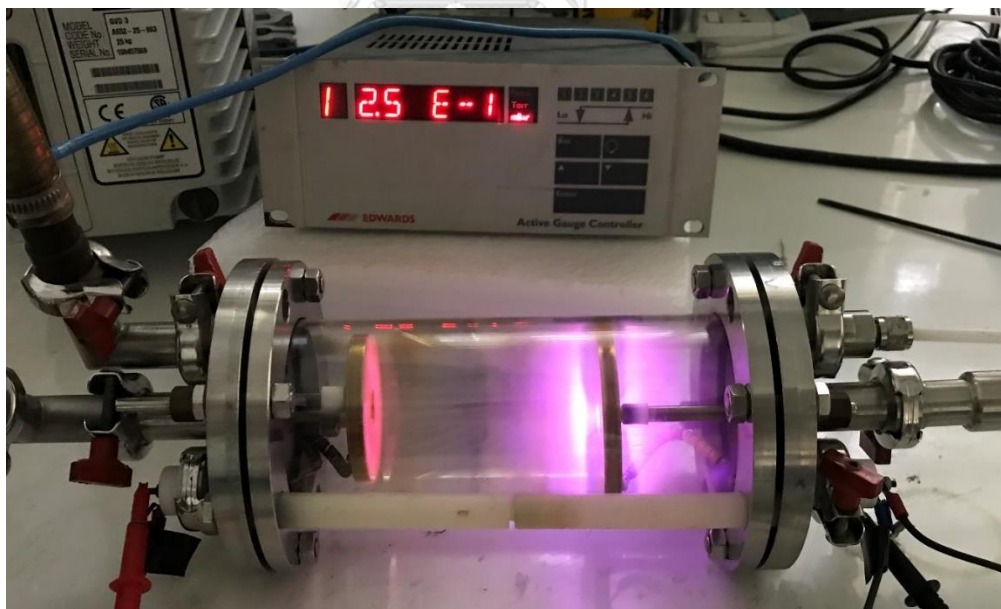


Figure 21 Argon plasma at 0.25 mbar

3.5 THE CONSTRUCTED LANGMUIR PROBE

The components of the constructed Langmuir probe are divided into 3 parts, which are a metal tip which is made of tungsten, the metal conductor rod is made of copper, and an insulator is made of Teflon. The constructed probe tip has an outer diameter of 1.6 millimeters and the outer diameter of the insulator is 5 millimeters. The probe schematics, prototype, and measurement system are shown in Figures 22, 23, and 24.

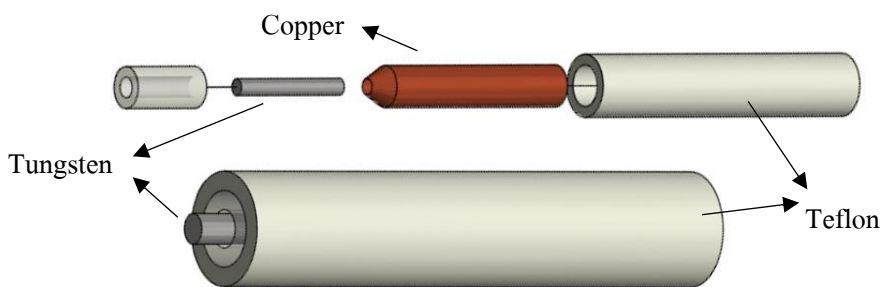


Figure 22 Schematics diagram of Langmuir probe

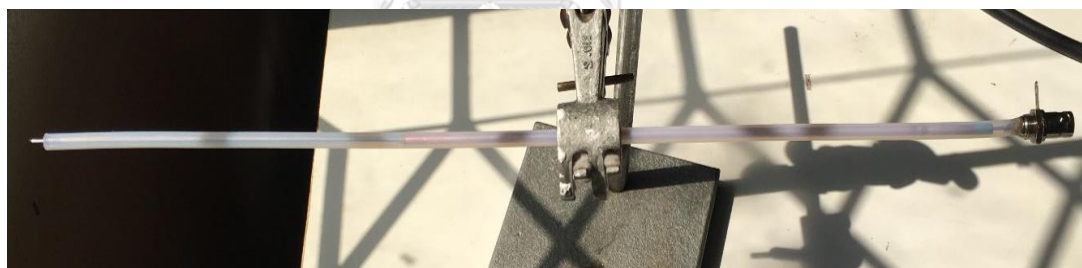


Figure 23 Langmuir probe prototype with BNC conductor

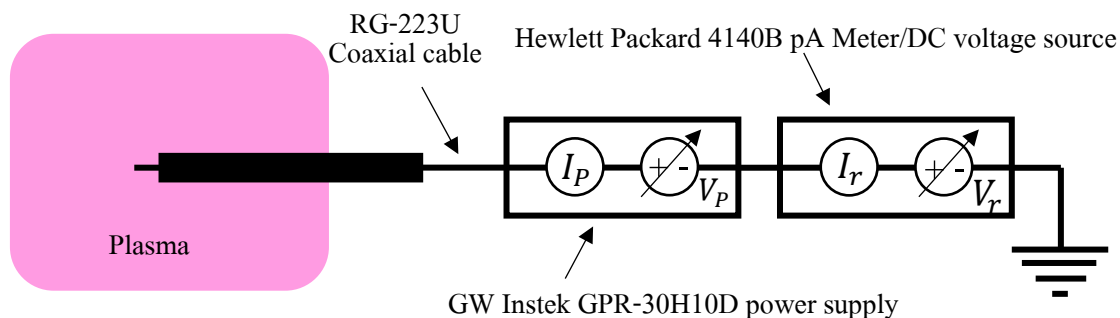


Figure 24 Langmuir probe measurement system

The constructed Langmuir probe with female BNC connector was connected with Hewlett Packard 4140B pA Meter/DC voltage source by using RG-223U coaxial cable with male to male BNC connector to obtain the I-V characteristics. The device can generate a potential range of -100 to 100 V. Practically, the device needs to be connected to GW Instek GPR-30H10D power supply to be able to obtain the total I-V characteristics. The picture of Hewlett Packard 4140B pA Meter/DC voltage source, GW Instek GPR-30H10D power supply, RG-223U coaxial cable, and BNC connector are shown in Figure 25.



Figure 25 Langmuir probe Equipment

(a) GW Instek GPR-30H10D power supply

(b) Male and Female BNC connector

(c) RG-223U coaxial cable

(d) Hewlett Packard 4140B pA Meter/DC

voltage source

3.6 LANGMUIR PROBE MEASUREMENT

The constructed Langmuir probe was connected with Hewlett Packard 4140B pA Meter/DC voltage source to obtain the I-V characteristics and the plasma parameter. The experimental results which are the I-V characteristic example and the plasma densities at any DC generated power is shown in Figure 26 and Figure 27.

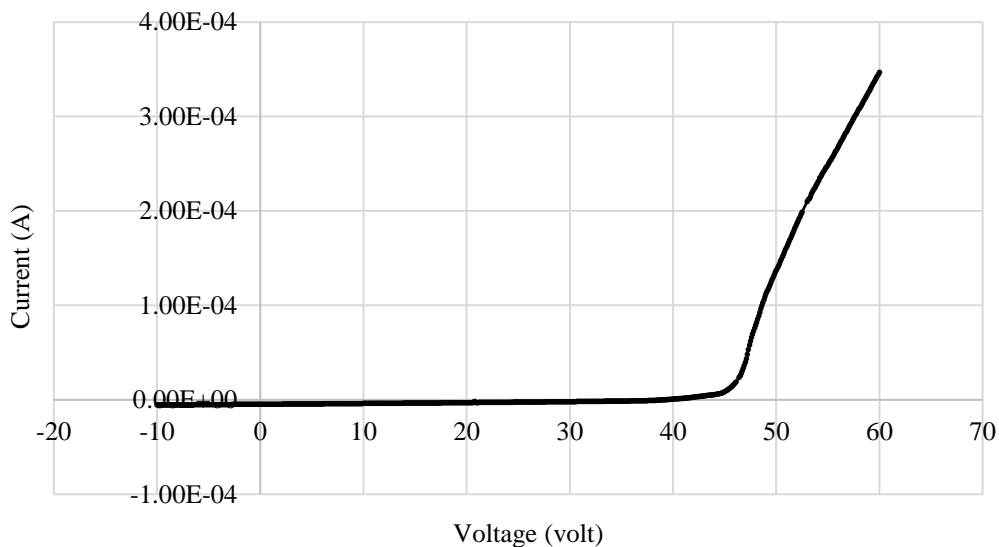


Figure 26 The I-V characteristic example at power 2.055 watts that obtained from DC plasma by using the constructed Langmuir probe at any DC generated power

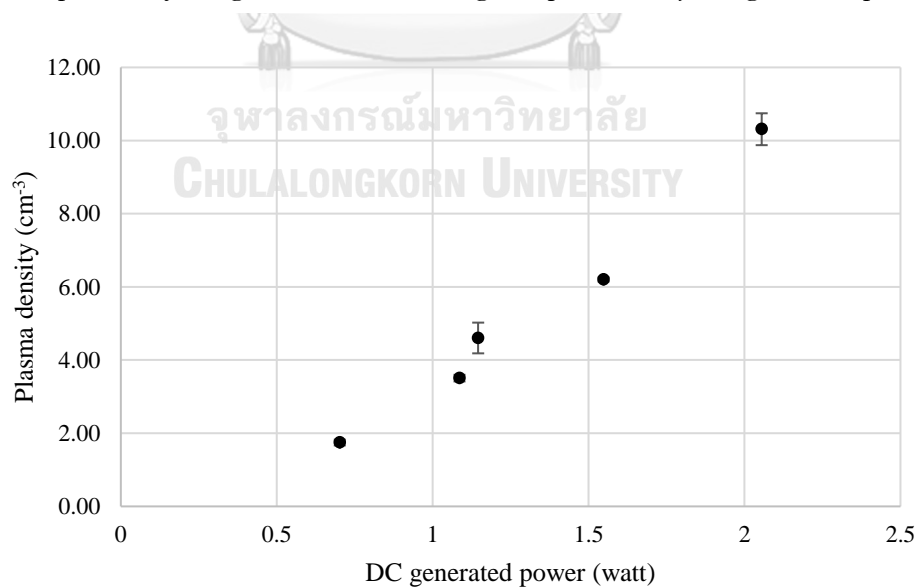


Figure 27 The plasma densities are obtained from the DC plasma by using the constructed Langmuir probe at any DC generated power

According to Figure 26, and 27, It can be summarized as a Table 1. as follows:

DC generated power (watt)	Plasma density (10^9 cm^{-3})			
	Data set	Data	Average	Standard deviation
0.702	1	1.68	1.75	0.079
	2	1.83		
	3	1.73		
1.086	1	3.52	3.51	0.091
	2	3.59		
	3	3.41		
1.146	1	4.81	4.60	0.420
	2	4.88		
	3	4.12		
1.548	1	6.14	6.20	0.057
	2	6.22		
	3	6.25		
2.055	1	10.61	10.31	0.436
	2	9.81		
	3	10.51		

Table 1 Summary table of plasma densities
from DC plasma measurement by using Langmuir probe

4. ACTIVE PLASMA RESONANCE SPECTROSCOPY

4.1 CHAPTER OVERVIEW

This chapter presents the details on active plasma resonance spectroscopy (APRS). From past to present, the Langmuir probe is a popular and traditional method. However, the probe must be inserted directly into the plasma which leads to disadvantages in unavoidable plasma perturbation and the probe contamination due to the sputtered metal molecules from the tip. The APRS is one of the plasma diagnostic methods for measuring plasma parameters as the probe tip will not directly contact the plasma hence does not cause contamination. To study the plasma parameter by using APRS, it is necessary to use high frequencies. At high frequencies, the wavelength is much smaller than the circuit size. A quasi-static circuit theory cannot be applied. Therefore, we need to use the transmission line theory [19]. In order to find the solution of the transmission line resonator and the relation with the plasma density, the details of the lossless transmission line, transmission line resonator is shown in this chapter.

4.2 TRANSMISSION LINE THEORY

As already stated above, a quasi-static circuit theory cannot be applied at high frequencies. Therefore, we need to use the transmission line theory. In order to find the solution of the transmission line, we consider the transmission line as a model which is a lumped-element circuit as shown in Figure 28. Consider a short section ΔZ of a transmission line, the lumped-element circuit consists of 4 components which are resistance per unit length, inductance per unit length, conductance per unit length, and capacitance per unit length [19].

where R is the resistance per unit length (Ω/m)
 L is the inductance per unit length (H/m)
 G is the conductance per unit length (S/m)
 C is the capacitance per unit length (F/m)
 ΔZ is the length of the transmission line (m)
 v is the electric voltage (V)
 i is the electric current (A)

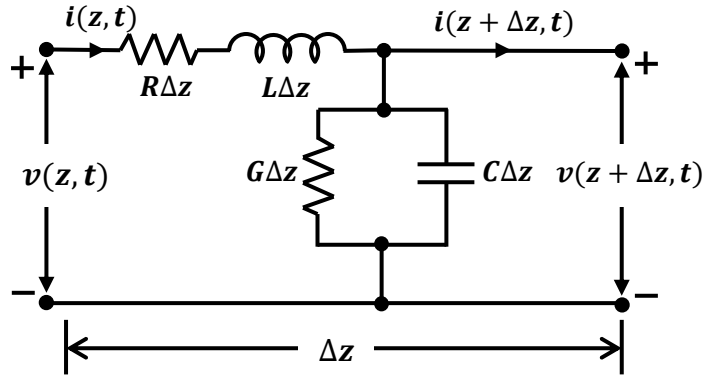


Figure 28 Lumped-element equivalent circuit of a transmission line section

Using Kirchhoff's Voltage Law and Kirchhoff's Current Law circuit theorems, we can derive the following differential equations for this section of the transmission line. [19]

$$v(z, t) - R\Delta z i(z, t) - L\Delta z \frac{\partial i(z, t)}{\partial t} - v(z + \Delta z, t) = 0 \quad (33.1)$$

$$i(z, t) - G\Delta z v(z + \Delta z, t) - C\Delta z \frac{\partial v(z + \Delta z, t)}{\partial t} - i(z + \Delta z, t) = 0 \quad (33.2)$$

Let $\Delta z \rightarrow 0$ and apply Taylor's expansion

$$-\frac{\partial v(z, t)}{\partial z} = Ri(z, t) + L \frac{\partial i(z, t)}{\partial t} \quad (34.1)$$

$$-\frac{\partial i(z, t)}{\partial z} = Gv(z, t) + C \frac{\partial v(z, t)}{\partial t} \quad (34.2)$$

For sinusoidal varying voltages and currents, we can use phasor forms where j is complex number.

$$v(z, t) = \text{Re}\{V(z)e^{j\omega t}\} \quad (35.1)$$

$$i(z, t) = \text{Re}\{I(z)e^{j\omega t}\} \quad (35.2)$$

$V(z)$ and $I(z)$ are called phasors of $v(z, t)$ and $i(z, t)$. In terms of phasors, the coupled equations can be written as:

$$-\frac{dV(z)}{dz} = (R + j\omega L)I(z) \quad (36.1)$$

$$-\frac{dI(z)}{dz} = (G + j\omega C)V(z) \quad (36.2)$$

After decoupling,

$$\frac{d^2V(z)}{dz^2} = \gamma^2 V(z) \quad (37.1)$$

$$\frac{d^2I(z)}{dz^2} = \gamma^2 I(z) \quad (37.2)$$

The solutions of the voltage and current in a transmission line are

$$V(z) = V_0^+ \exp(-\gamma z) + V_0^- \exp(\gamma z) \quad (38.1)$$

$$I(z) = I_0^+ \exp(-\gamma z) + I_0^- \exp(\gamma z) \quad (38.2)$$

where
$$\gamma = \alpha + i\beta = \sqrt{(R + i\omega L)(G + i\omega C)} \quad (39)$$

and it is called the complex propagation constant

where α is attenuation constant (Np/m)

β is phase constant (rad/m)

V_0^+, I_0^+ is wave amplitudes in the forward directions at $z = 0$

V_0^-, I_0^- is wave amplitudes in the backward directions at $z = 0$

According to the coupled transmission line equation (34.1, 34.2)

$$I(z) = \frac{\gamma}{R - i\omega L} (V_0^+ \exp(-\gamma z) - V_0^- \exp(\gamma z)) \quad (40)$$

Define characteristics impedance Z_0

$$Z_0 = \frac{R - i\omega L}{\gamma} = \sqrt{\frac{R - i\omega L}{G - i\omega C}} \quad (41)$$

Define reflection coefficient at $z = 0$

$$\Gamma = \frac{\text{reflection voltage at } z=0}{\text{incident voltage at } z=0} = \frac{V_0^-}{V_0^+} \quad (42)$$

where Γ is the reflection coefficient

The relation between reflection coefficient and dissipated power is shown as equation [19]

$$S(\omega) \propto (1 - |\Gamma|^2) \quad (43)$$

where $S(\omega)$ is dissipated power

4.3 LOSSLESS TRANSMISSION LINE

The lossless transmission line is a transmission line model without resistance R and conductance G per unit length ($R = G = 0$) [19]. The complex propagation constant and characteristics impedance are then

$$\gamma = i\omega\sqrt{LC} = i\omega\sqrt{\mu\epsilon} = i2\pi f\sqrt{\mu\epsilon} = i\frac{2\pi}{\lambda} \quad (44)$$

$$Z_0 = \sqrt{\frac{L}{C}} \quad (45)$$

where λ is wavelength along the transmission line and defined as

$$\lambda = \frac{1}{f\sqrt{\mu\epsilon}} \quad (46)$$

In terms of the reflection coefficient Γ , the total voltage and current can be written as

$$V(z) = V_0^+ e^{-\gamma z} (1 + \Gamma_L e^{2\gamma z}) \quad (47.1)$$

$$I(z) = I_0^+ e^{-\gamma z} (1 - \Gamma_L e^{2\gamma z}) \quad (47.2)$$

For an infinitely long transmission line, there is no reflected wave (backward traveling wave). So, there is only a forward traveling wave [19].

$$Z(z) = \frac{V(z)}{I(z)} = \frac{V_0^+}{I_0^+} = Z_0 \quad (48)$$

$$\Gamma_L = 0 \quad (49)$$

When lossless transmission line terminated by impedance load Z_L at $z = 0$

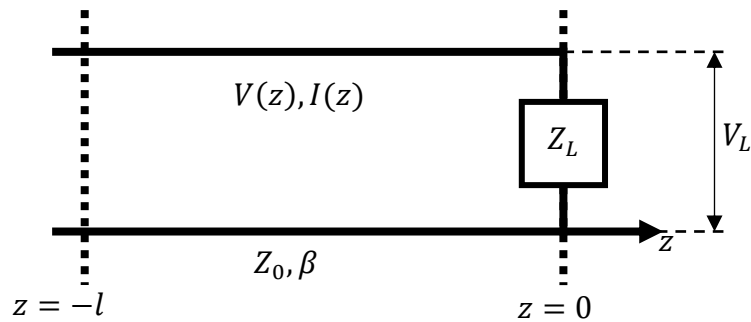


Figure 29 A lossless transmission line terminated by a Z_L impedance load

In the z coordinate system,

$$V(z) = V_0^+ e^{-\gamma z} + V_0^- e^{\gamma z} \quad (50.1)$$

$$I(z) = I_0^+ e^{-\gamma z} + I_0^- e^{\gamma z} \quad (50.2)$$

At the position of load ($z = 0$), the reflection coefficient, the voltage and the current are

$$\Gamma(z = 0) = \frac{V_0^-}{V_0^+} = \Gamma_L \quad (51)$$

$$\frac{V_L}{I_L} = Z_L \quad (52)$$

where

$$V_0^+ + V_0^- = V_L \quad (53.1)$$

$$\frac{V_0^+}{Z_0} - \frac{V_0^-}{Z_0} = I_L \quad (53.2)$$

Solve these two equations, we have:

$$V_0^+ = \frac{1}{2} I_L (Z_L + Z_0) \quad (54.1)$$

$$V_0^- = \frac{1}{2} I_L (Z_L - Z_0) \quad (54.2)$$

The reflection coefficient (Γ) and the impedance load (Z_L),

$$\Gamma_L = \frac{V_0^-}{V_0^+} = \frac{Z_L - Z_0}{Z_L + Z_0} \quad (55)$$

then,

$$Z_L = \frac{V_0^+ + V_0^-}{V_0^+ - V_0^-} Z_0 \quad (56)$$

4.4 TRANSMISSION LINE RESONATOR

In the previous section, the solutions of the transmission line were used to realize the resonance in the transmission line. The length of a loaded transmission line can affect a load impedance of the transmission line resonator. In order to find the resonance condition, the transmission line with finite length load can be considered in 2 cases which are short and open circuit. Consider a transmission line with a finite length l loaded with Z_L as a single load [19] as shown in Figure 30.

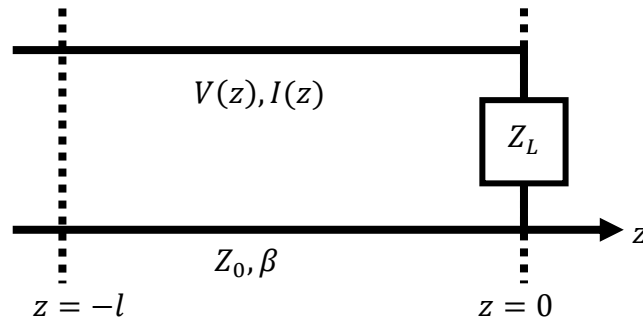


Figure 30 A transmission line with a finite length l with Z_L as a single load

In the $z = -l$ coordinate system,

$$V(-l) = V_0^+ e^{\gamma l} + V_0^- e^{-\gamma l} \quad (57.1)$$

$$I(-l) = I_0^+ e^{\gamma l} + I_0^- e^{-\gamma l} \quad (57.2)$$

As we know by solving the two equations (53.1) and (53.2) with $l \neq 0$,

$$V_0^+ e^{\gamma l} = \frac{1}{2} I(-l) (Z(-l) + Z_0) \quad (58.1)$$

$$V_0^- e^{-\gamma l} = \frac{1}{2} I(-l) (Z(-l) - Z_0) \quad (58.2)$$

$$\Gamma(l) = \frac{\text{reflection voltage at point } l}{\text{incident voltage at point } l} = \frac{V_0^- e^{-\gamma l}}{V_0^+ e^{\gamma l}} = \frac{Z(-l) - Z_0}{Z(-l) + Z_0} = \Gamma_L e^{-2\gamma l} \quad (59)$$

then,
$$Z(-l) = Z_0 \frac{1 + \Gamma(-l)}{1 - \Gamma(-l)} \quad (60)$$

According to equation (44), (58.1), (58.2), (59), and (60), the impedance of the loaded transmission line with length l are

$$Z(-l) = \frac{V(-l)}{I(-l)} = Z_0 \left(\frac{\exp\left(-i\frac{2\pi}{\lambda}l\right) + \Gamma_L \exp\left(i\frac{2\pi}{\lambda}l\right)}{\exp\left(-i\frac{2\pi}{\lambda}l\right) - \Gamma_L \exp\left(i\frac{2\pi}{\lambda}l\right)} \right) \quad (61)$$

where Γ_L is the reflection coefficient at $z = 0$ defined as

$$\Gamma_L = \frac{Z_L - Z_0}{Z_L + Z_0} \quad (62)$$

Resonances occur when the impedance is vanished [19]. The conditions for the open-circuited transmission line resonators are $\frac{l}{\lambda} = \frac{1}{2}(n - \frac{1}{2})$ when n are positive integers [19], While the conditions for the short-circuited transmission line resonators are $\frac{l}{\lambda} = \frac{n}{2}$ where n are positive integers. The transmission line resonance frequency is

$$f = \frac{1}{\lambda\sqrt{LC}} \quad (63)$$

For the open-circuited transmission line, the resonance frequency is

$$f = \frac{1}{2l} \left(n - \frac{1}{2}\right) \frac{1}{\sqrt{\mu\epsilon}} \quad (64)$$

The first resonance frequency of a specific medium ($n = 1$) is

$$f = \frac{1}{4l} \frac{c}{\sqrt{\mu_r \epsilon_r}} \quad (65)$$

$$c = \frac{1}{\sqrt{\mu_0 \epsilon_0}} \quad (66)$$

where

c is the speed of light

μ_r is the relative permeability of a specific medium

ϵ_r is the relative permittivity of a specific medium

μ_0 is the permeability of vacuum which is equal to $4\pi \times 10^{-7} \text{ N} \cdot \text{A}^{-2}$

ϵ_0 is the permittivity of vacuum which is equal to $8.8542 \times 10^{-12} \text{ F} \cdot \text{m}^{-1}$

When the medium in the resonator is changed the resonance frequencies also change, consider the ratio of the first resonance frequencies between vacuum and arbitrary medium.

$$\frac{f_0}{f} = \sqrt{\mu_r \epsilon_r} \quad (67)$$

For the vacuum, $\mu_r = 1$

$$\frac{f_0}{f} = \sqrt{\epsilon_r} \quad (68)$$

The relative permittivity of a collisionless plasma is

$$\epsilon_r = 1 - \frac{\omega_{pe}^2}{\omega^2} \quad (69)$$

According to equation (69), equation (68) becomes

$$\frac{f_0}{f} = \sqrt{1 - \left(\frac{n_e e^2}{2\pi\epsilon_0 m_e f}\right)^2} \quad (70)$$

Finally, the plasma electron density is

$$n_e = (2\pi)^2 \frac{\epsilon_0 m_e}{e^2} (f^2 - f_0^2) \quad (71)$$

According to the equation (68), and (70) the plasma density in equation (71) becomes

$$n_e = (2\pi)^2 \frac{\epsilon_0 m_e}{e^2} (f_{pe}^2) \quad (72)$$



5. HEMISPHERE PROBE

5.1 CHAPTER OVERVIEW

This chapter presents the solution details of APRS in the hemisphere shape and the dissipated power simulation. The multipole resonance probe is the name-calling the APRS in a hemisphere shape. The name of the multipole resonance probe comes from an analysis of the solution of electrostatic potential by using multipole expansion. The solution of the hemisphere probe is one possible way to find the electrostatic potential mathematical model by solving the Laplace equation in the spherical coordinate. The electrostatic potential can lead to the dissipated power calculated using the MATLAB simulation program. The detail of the dissipated power simulation is shown in the last section of this chapter.

5.2 HEMISPHERE PROBE SOLUTION

As already stated above, the solution of the hemisphere probe is the one possible way to find the electrostatic potential mathematical model. The hemisphere probe consists of a conducting sphere cut into two hemispheres and insulated each other by using a thin dielectric sheet [16]. The schematic diagram is shown in Figure 31.

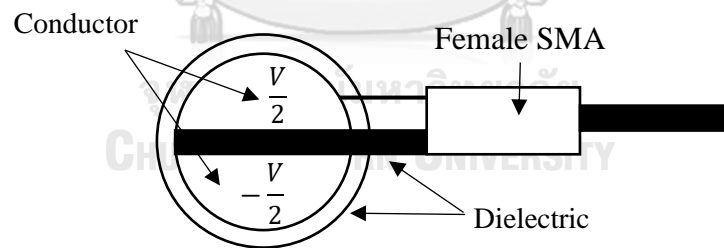


Figure 31 Schematic diagram of the hemisphere probe

In the study of plasma density by using a hemisphere probe, a method for determining the plasma density was proposed by Martin Lapke in 2008 [9]. The probe was considered based on cold plasma condition whereas the current in the plasma is carried by displacement of the electrons alone and ions are too heavy to follow. The electrostatic approximation can then be used [7].

$$\vec{E} = -\nabla\Phi \quad (73)$$

The electrostatic potential can be obtained by solving the Laplace equation in the spherical coordinate with azimuthal symmetry as shown the equation

$$\nabla^2 \Phi = 0 \quad (74)$$

In spherical coordinates, the electrostatic potential with azimuthal symmetry obeys [20]

$$\frac{1}{r^2} \frac{\partial}{\partial r} \left(\epsilon_r r^2 \frac{\partial \Phi}{\partial r} \right) + \frac{1}{r^2 \sin \theta} \frac{\partial}{\partial \theta} \left(\epsilon_r \sin \theta \frac{\partial \Phi}{\partial \theta} \right) = 0 \quad (75)$$

The solution of the Laplace equation in spherical coordinate can be written as [21, 22]

$$\Phi^i(r, \theta) = \sum_{s=1}^{\infty} (A_s^i r^{2s-1} + B_s^i r^{-2s}) P_{2s-1}(\cos \theta) \quad (76)$$

The boundary conditions for two symmetrically driven hemispheres as

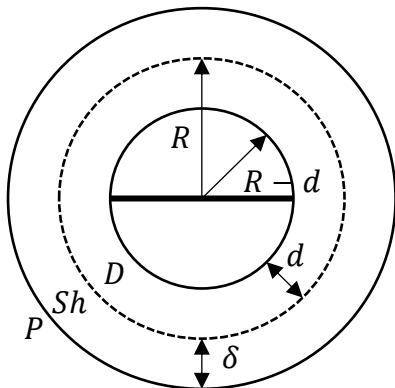
$$\Phi_{r=R-d} = \begin{cases} \frac{V}{2}, & 0 \leq \theta \leq \frac{\pi}{2} \\ -\frac{V}{2}, & \frac{\pi}{2} \leq \theta \leq \pi \end{cases} \quad (77.1)$$

and

$$\Phi_{r \rightarrow \infty} = 0 \quad (77.2)$$

We considered an idealized case where the cable was neglected, and the two metal hemispheres were insulated from each other by a dielectric of negligible thickness. They were surrounded by a dielectric coating of thickness d and a plasma sheath of thickness δ . The electrodes thus form an exact sphere of radius $R - d$. The plasma was taken to have a constant electron density (n_e) and constant plasma frequency.

In order to give explicit values for the electrostatic potential of the hemisphere probe, it is necessary to divide the area into 3 regions, which are plasma, plasma sheath, and dielectric, as shown in Figure 32. The potential distinguishes the three media by an index i which can be replaced by plasma(P), plasma sheath(Sh), and dielectric(D),



The equation can be written as

$$\text{Plasma}(P) \quad r > R + \delta \quad (78)$$

$$\text{Plasma Sheath}(Sh) \quad R < r < R + \delta \quad (79)$$

$$\text{Dielectric}(D) \quad R - d < r < R \quad (80)$$

Figure 32 The hemisphere probe regions

Representing the boundary conditions in various areas into the relationship

$$\text{Plasma} \quad \Phi^P(r, \theta) = \sum_{s=1}^{\infty} (B_s^P r^{-2s}) P_{2s-1}(\cos\theta) \quad (81.1)$$

$$\text{Plasma Sheath} \quad \Phi^{sh}(r, \theta) = \sum_{s=1}^{\infty} (A_s^{sh} r^{2s-1} + B_s^{sh} r^{-2s}) P_{2s-1}(\cos\theta) \quad (81.2)$$

$$\text{Dielectric} \quad \Phi^D(r, \theta) = \sum_{s=1}^{\infty} (A_s^D r^{2s-1} + B_s^D r^{-2s}) P_{2s-1}(\cos\theta) \quad (81.3)$$

where $A_s^{sh}, B_s^{sh}, A_s^D, B_s^D$ and B_s^P are constants.

Electric displacement (\vec{D}) in dielectric can be written as an electric field (\vec{E}) as the equation

$$\vec{D} = \epsilon \vec{E} \quad (82)$$

The relationship between the electric potential (Φ) and the electric field (\vec{E}) with the variable r can be written as following [20]

$$E_r = -\frac{\partial \Phi}{\partial r} \quad (83)$$

$$\text{where} \quad \frac{\partial \Phi}{\partial r} = \sum_{s=1}^{\infty} (A_s^i (2s-1) r^{2s-2} + B_s^i (-2s) r^{-2s-1}) P_{2s-1}(\cos\theta) \quad (84)$$

Consider the continuity of the electric displacement, it was found that there is continuity in the perpendicular direction between the medium which can be written in the equation [23]

$$D_{\perp}^{sh}(r=R) = D_{\perp}^D(r=R) \quad (85)$$

$$D_{\perp}^{sh}(r=R+\delta) = D_{\perp}^P(r=R+\delta) \quad (86)$$

Define $(BDC)_n$ as the boundary condition of the n^{th} Legendre polynomial. From Legendre Polynomial Orthogonality, it possible to write equation (81.3) as

$$(BDC)_n = \int_{-1}^1 \Phi^D(r=R-d, \theta) P_{2n-1}(\cos\theta) d(\cos\theta) \quad (87.1)$$

$$(BDC)_n = (A_n^D (R-d)^{2n-1} + B_n^D (R-d)^{-2n}) \frac{2}{4n-1} \quad (87.2)$$

Substitute the boundary conditions of the conductor (77.1) into the relation (87.1) as

$$(BDC)_n = V \int_0^1 P_{2n-1}(x) dx \quad (88)$$

From the equation (87.2) can be rewritten as follows

$$B_n^D (A_n^D) = \left[BDC \left(\frac{4n-1}{2} \right) - A_n^D (R-d)^{2n-1} \right] (R-d)^{2n} \quad (89)$$

Consider that the electric potential is continuous, that is the edge of plasma sheath potential and the edge of plasma potential is continuous. The potential at the edge of the plasma sheath is equal to the potential at the edge of the plasma which can be written as equation (90) and (91) respectively.

$$\Phi^{sh}(r = R + \delta) = \Phi^P(r = R + \delta)$$

$$A_s^{sh}(R + \delta)^{2s-1} + B_s^{sh}(R + \delta)^{-2s} = B_s^P(R + \delta)^{-2s} \quad (90)$$

$$\Phi^{sh}(r = R) = \Phi^D(r = R)$$

$$A_s^{sh}R^{2s-1} + B_s^{sh}R^{-2s} = A_s^D R^{2s-1} + B_s^D R^{-2s} \quad (91)$$

Substitute the equation (84) into the equation (82) when $P_{2s-1} \cos(\theta)$ has linearly independent

$$\epsilon_0 \epsilon_D (A_s^D (2s-1)R^{2s-2} + B_s^D (-2s)R^{-2s-1}) = \epsilon_0 (A_s^{sh} (2s-1)R^{2s-2} + B_s^{sh} (-2s)R^{-2s-1}) \quad (92)$$

Substitute the equation (82) into the equation (76) where ϵ_P is the electric permittivity of plasma

$$\epsilon_0 (A_s^{sh} (2s-1)(R + \delta)^{2s-2} + B_s^{sh} (-2s)(R + \delta)^{-2s-1}) = \epsilon_0 \epsilon_P (B_s^P (-2s)(R + \delta)^{-2s-1}) \quad (93)$$

From the equation (92) and (93) can be rewritten as

$$R^{2s-1} A_s^{sh} + R^{-2s} B_s^{sh} + ((R - d)^{4n-1} R^{-2s} - R^{2s-1}) A_s^D = R^{-2s} \left(\frac{4s-1}{2} \right) (BDC)_s \quad (94)$$

$$(R + \delta)^{2s-1} A_s^{sh} + (R + \delta)^{-2s} B_s^{sh} - (R + \delta)^{-2s} B_s^P = 0 \quad (95)$$

$$\begin{aligned} (2s-1)R^{2s-2} A_s^{sh} + (-2s)R^{-2s-1} B_s^{sh} - \epsilon_D [(2s-1)R^{2s-2} - (-2s)R^{2s-1}(R-d)^{4s-1}] A_s^D \\ = \epsilon_D (-2s)R^{2s-1}(R-d)^{2s} \left(\frac{4s-1}{2} \right) (BDC)_s \end{aligned} \quad (96)$$

$$(2s-1)(R + \delta)^{2s-2} A_s^{sh} + (-2s)(R + \delta)^{-2s-1} B_s^{sh} - \epsilon_P (-2s)(R + \delta)^{-2s-1} B_s^P = 0 \quad (97)$$

Equation (93) to (96) can be rewritten in matrix forms:

$$\begin{bmatrix} R^{2s-1} & R^{-2s} & (R-d)^{4s-1}R^{-2s} - R^{2s-1} & 0 & \begin{bmatrix} A_s^{sh} \\ B_s^{sh} \\ A_s^D \\ B_s^D \end{bmatrix} \\ (R+\delta)^{2s-1} & (R+\delta)^{-2s} & 0 & -(R+\delta)^{-2s} & \\ (R+\delta)^{2s-2} & (-2s)R^{2s-1} & \epsilon_D [(-2s)(R-d)^{4s-1}R^{-2s-1} - (2s-1)R^{2s-2}] & 0 & \\ (2s-1)(R+\delta)^{2s-2} & (-2s)(R+\delta)^{2s-1} & 0 & \epsilon_P (-2s)(R+\delta)^{-2s-1} & \end{bmatrix} \\ = \begin{bmatrix} R^{-2s}(\frac{4s-1}{2})(BDC)_s & & & & \\ \epsilon_D (-2s)R^{-2s-1}(R-d)^{2s}(\frac{4s-1}{2})(BDC)_s & 0 & & & \\ 0 & & & & \end{bmatrix} \quad (98)$$

Take the values A_s^{sh} , B_s^{sh} , A_s^D , B_s^D which obtained from the solution of the equation (98) and insert into the equation (81.1), (81.2), and (81.3) to find the electrostatic potential of each area around the probe (Φ). The dissipated power at different feeding frequency $S(\omega)$ can be calculated as the integral over the dissipation in the plasma [7].

$$S(\omega) = \int_p \frac{\epsilon_0 v \omega_{pe}^2}{2(v^2 + \omega^2)} |\nabla \Phi_p|^2 d^3r \quad (99)$$

The dissipated power in equation (99) shows that the relation between the match frequency (the frequency of highest dissipated power, ω) and the plasma frequency (ω_{pe}). Practically, it is too complicated to solve equations analytically. So, the dissipated power will be simulated by using the MATLAB program.

5.3 HEMISPHERE PROBE DISSIPATED POWER SIMULATION

From the solution of the hemisphere probe, as shown in the previous section, the simulation of the dissipated power was performed to find the match frequency corresponding to the specified plasma frequency. This section presents the flowchart for determining dissipated power using the MATLAB simulation program as shown in Figure 33. The simulation started by solving the Laplace equation to find the electrical potential of each region. The potential was shown in the equation (81.1) to (81.3). It can be seen that there are 5 constants which are A_S^{sh} , B_S^{sh} , A_S^D , B_S^D and B_S^P . The constants were collected by solving the equation (98). Then, the related parameters were defined and shown in Table 2. After that, the dissipated power can be found from the equation (99).

From the dissipated power simulation, the electrical potential around the hemisphere probe was collected. Using the electrical potential to create a hologram from $\theta = 0$ to π due to the hemisphere probe symmetry as shown in Figure 34. Additionally, the electrical potential was led to find the electric field around the hemisphere probe from the equation (73) and shown in Figure 35.

In order to find the solution of the dissipated power of the hemisphere probe, the order of Legendre polynomial must be defined. So, we need to find the appropriated order of the Legendre polynomial which is suitable for the simulation. The simulation of the n^{th} Legendre polynomial dissipated power shows that the match frequency was convergence when the order of Legendre polynomial was increased as shown in Figure 36. From the experiment, the simulations indicated that the dissipated power cannot be determined when the order was greater than 17. Therefore, the 17th Legendre polynomial was used for the most accurate results.

The values of plasma frequency ω_{pe} can be obtained from the frequency that exhibited the highest dissipated power (the lowest reflection coefficient) [7]. The frequency is called match frequency. Practically, we can inverse the experiment match frequencies to obtain the experiment plasma frequency by using the analytical solution of the hemisphere probe as shown in the equation (99). Finally, the plasma density which relates directly to plasma frequency can be realized from the equation (72).

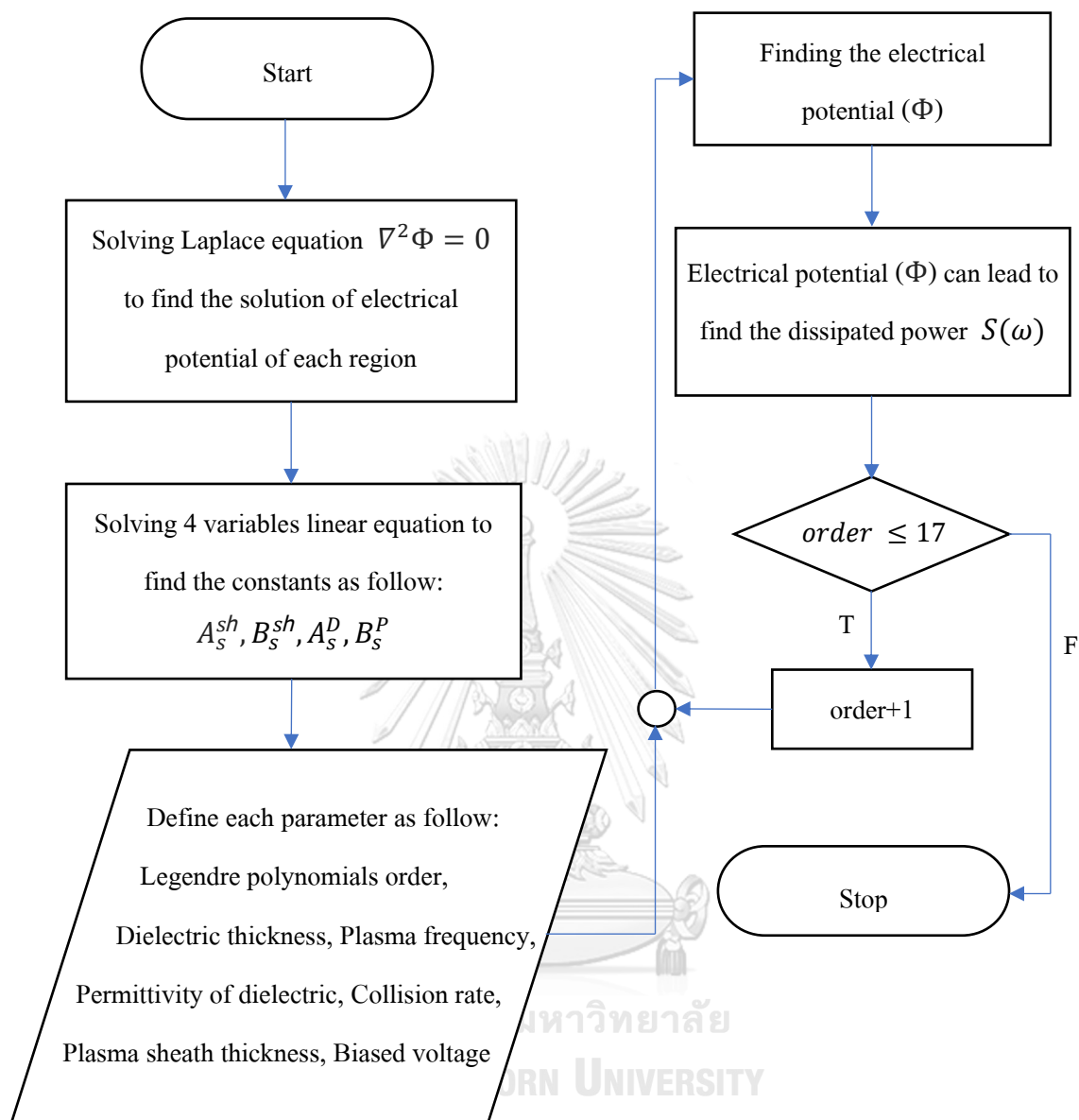


Figure 33 Flowchart for determining the simulation of dissipated power

Variables	Value
Legendre polynomial order	1-17
Electrical voltage	1 V
Dielectric thickness	0.5 mm.
Plasma sheath thickness	0.5 mm.
Collision rate of particle	0.015
Hemisphere probe radius	5 mm.
Dielectric permittivity	5.4

Table 2 The constants of various variables

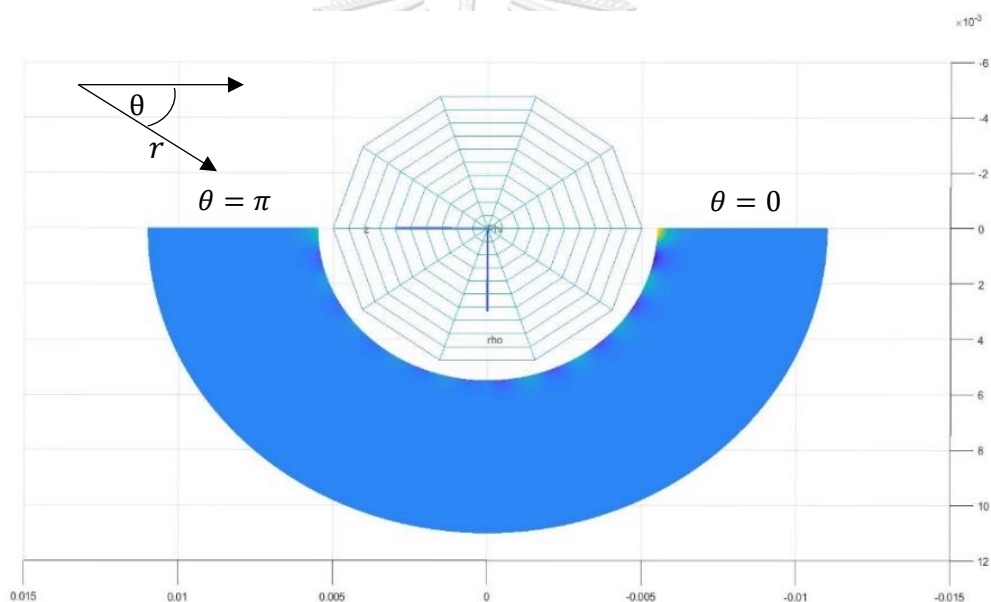


Figure 34 The simulation of the electrostatic potential at (r, θ) around the hemisphere probe

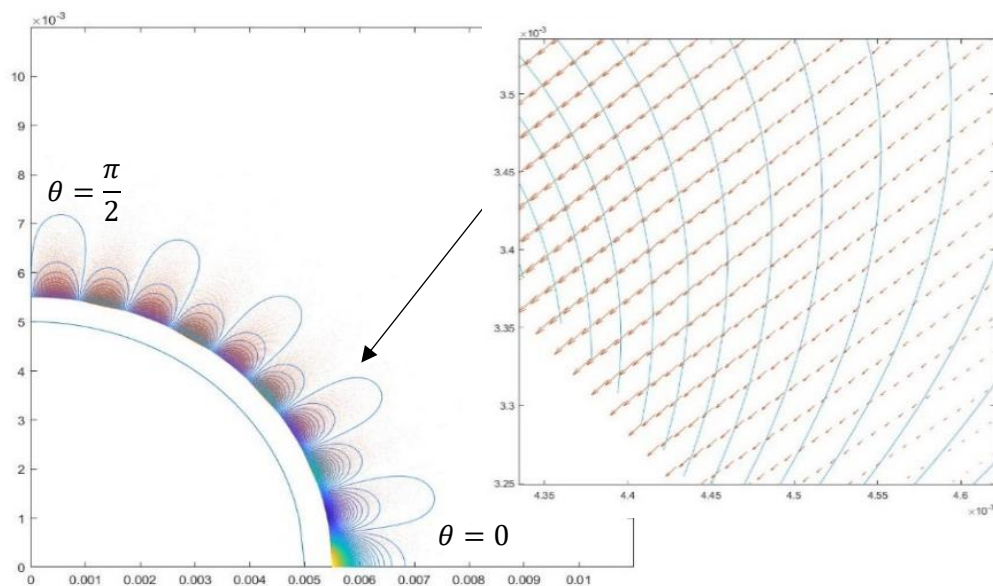


Figure 35 The simulation of the electric field at (r, θ) around the hemisphere probe

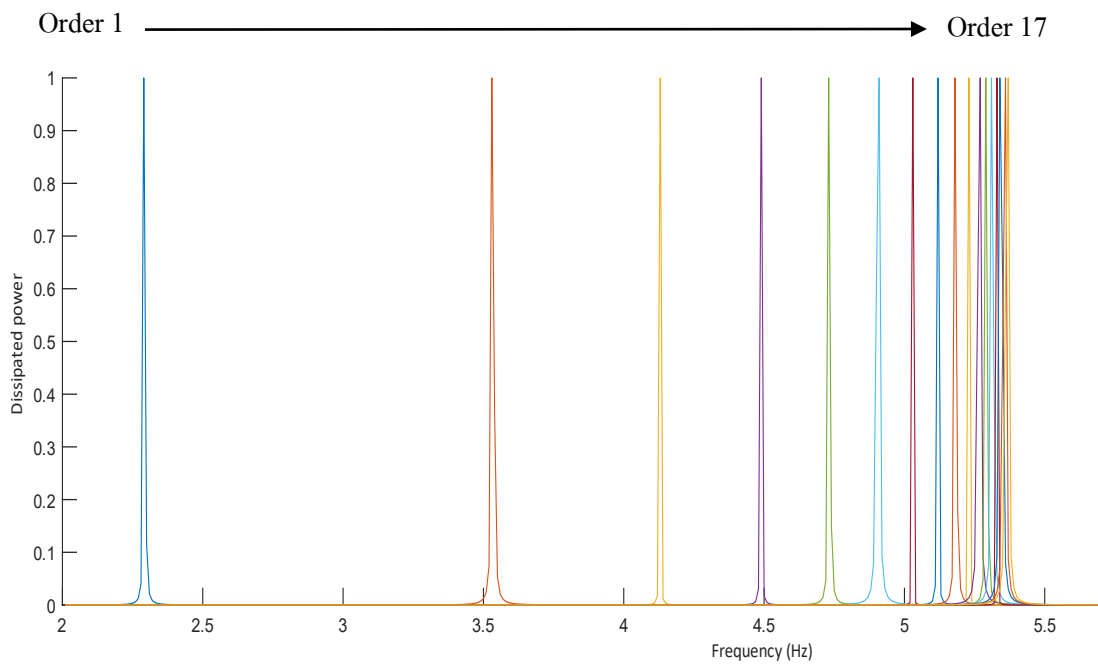


Figure 36 The simulation of the dissipated power at Legendre polynomial order 1 to 17

6. PROBE CONSTRUCTION AND MEASUREMENT SYSTEM

6.1 CHAPTER OVERVIEW

This chapter presents the details of the probe constructions and the plasma parameter measurement system. To study the plasma density, the plasma parameter measurements of the different probe tip shapes including hemisphere, microstrip, and parallel were constructed and performed to support the concept that the probe can be of any shape and does not need to be a hemisphere. The constructed probes were measured in the DC plasma system as well as the Langmuir probe. The probes were connected with the network analyzer. In the experiment, the system's reflection coefficient spectrum in the decibel scale was measured to obtain the match frequency which can lead to determining the plasma density. The first three sections of this chapter give the details on the characteristics of any probe shapes. The equipment and the measurement setup are shown in the last section of this chapter.

6.2 HEMISPHERE PROBE

As already stated above, the constructed hemisphere probe was constructed. It consists of a conducting stainless-steel sphere cut into two hemispheres and insulated against each other by a thin dielectric sheet. The hemispheres are soldered to a microstrip line and all covered by an insulator epoxy. The probe outer diameter is 10 mm, and the length of the microstrip line is 16 mm. The end of the probe is a female SMA connector. The dimension of the probe was chosen by the limitation of our vacuum chamber. The probe simulation and prototype are shown in Figure 37.

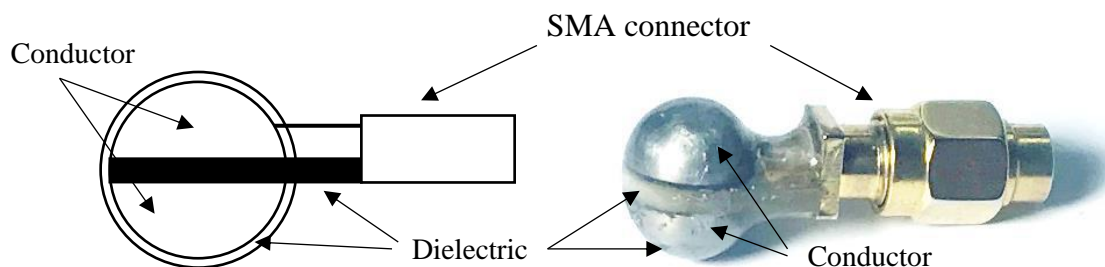


Figure 37 Schematics of hemisphere probe

6.3 MICROSTRIP PROBE

This section shows the constructed microstrip probe. The probe consists of a two-parallel conducting microstrip 3 millimeters wide and insulated against each other by a thin dielectric sheet. The probe is cover with an insulator which is made of borosilicate glass. The microstrip experiments conducted using 16 millimeters microstrip, and 21 millimeters microstrip. The prototypes of each length are shown in Figure 38.



Figure 38 (a) 16 millimeters microstrip and (b) 21 millimeters microstrip

6.4 PARALLEL PROBE

This section shows the constructed parallel probe. The probe consists of a two-parallel conducting rod 1-millimeter diameter and insulated against each other. The probe is cover with an insulator which is made of borosilicate glass. The parallel experiments were conducted using 16 millimeters parallel rod, and 21 millimeters parallel rod. The prototypes of each length are shown in Figure 39.



Figure 39 (a) 16 millimeters parallel, and (b) 21 millimeters parallel

6.5 MEASUREMENT SYSTEM

In order to find the plasma parameter by using the constructed probe including hemisphere, microstrip, and parallel probe, the probes need to connect with the Agilent E5071C ENA Vector Network Analyzer by using RG-142 coaxial cable to measure the reflection coefficient. A network analyzer is an instrument that commonly measures the scattering parameters of electrical networks because the reflection and transmission of electrical networks are easy to measure at high frequencies. In the experiment, the network analyzer which is the E5071C ENA Vector manufactured by Agilent Technologies. The device can measure a range of 9kHz to 20 GHz. There are 2 connection ports. In this project, the device was used to measure the scattering parameter (Γ). The characteristics of the device are shown in Figure 40.



Figure 40 E5071C ENA Vector Network Analyzer

The network analyzer can analyze many types of scattering parameter as follows:

S_{11} or reflection coefficient is the output signal via connection port 1 and receives the signal via connection port 1, which can indicate the value that how much signal is reflected from the system.

S_{12} is the frequency analyzer which will send the signal through the connection port 1 and receive the signal via the connection port 2, which is a value indicating that how much the signal can be transferred from the port 1 to port 2.

S_{21} is the frequency analyzer which will send the signal through the connection port 2 and receive the signal via the connection port 1, which is a value indicating that how much the signal can be transferred from the port 2 to port 1.

S_{22} or reflection coefficient is that the outputs signal via connection port 2 and receives the signal via connection port 2, which can indicate the value that how much signal is reflected from the system.

The connection between the probes and the network analyzer requires a male N-type to female SMA Adaptors because the network analyzer port is N-type, but the port of the probes is SMA. The pictures of pressure gauge, mass flow controller, RG-142 coaxial cable, and male N-type to female SMA Adaptors are shown in Figure 41.



Figure 41 The type of connector

(a) male N-type to female SMA adaptors

(b) RG-142 coaxial cable assembled with male SMA connectors on both ends

In the APRS probe experiments, the probes must be connected to port number one of the network analyzer to measure the reflection coefficient. The frequency that makes the lowest reflection coefficient, can be calculated for the plasma density of the plasma system. The probes measurement system is shown in Figure 42.

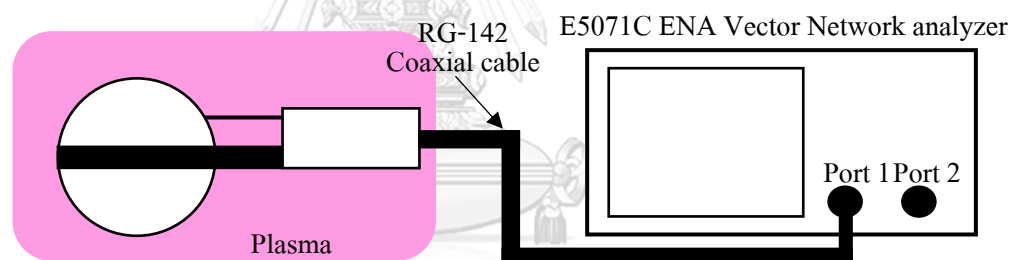


Figure 42 The probes measurement system

To compare the plasma density results, the hemisphere APRS probes and the Langmuir probe were measured simultaneously at the same location within the DC argon plasma discharge chamber as shown in Figure 43. The results of both methods will be compared. The system of plasma density measurement is shown in Figure 44. The studied plasma was ignited in the vacuum chamber to control the internal pressure.

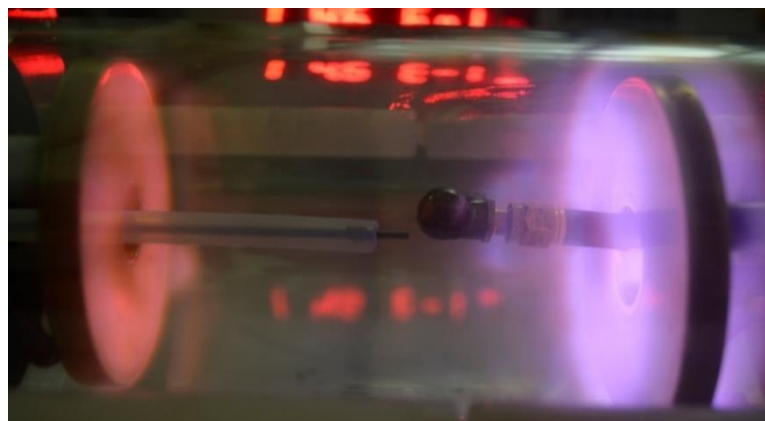


Figure 43 Hemisphere probe and Langmuir probe were measured simultaneously at the same location

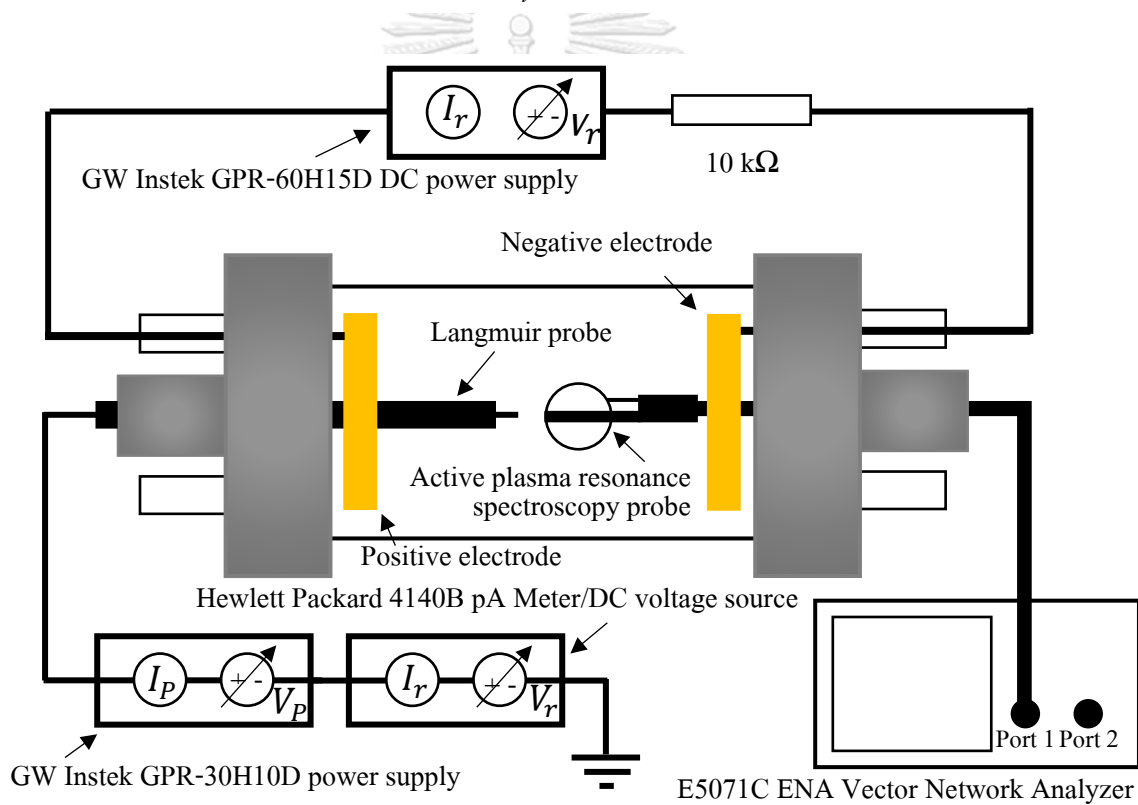


Figure 44 The system of plasma density measurement

7. PROBE MEASUREMENTS

7.1 CHAPTER OVERVIEW

This chapter presents the reflection coefficient results of APRS probes measurement at any DC generated power. The probes including the hemisphere probe, microstrip probe, and parallel probe were used to measure the match frequency which is the lowest reflection coefficient location (the highest dissipated power) by connecting to a network analyzer. The match frequencies of any probe will be calibrated by using the Langmuir probe plasma density as shown in chapter 8. Next, the hemisphere probe was the only one that has an analytical solution. The solution of the hemisphere probe was used to determine the plasma density by using the analytical solution of the hemisphere probe as shown in chapter 5. The collected hemisphere probe plasma densities were compared to the Langmuir plasma density. The comparison result was shown in the hemisphere section 7.1 of this chapter.

7.1 HEMISPHERE PROBE MEASUREMENT

To study the plasma parameter by using the hemisphere probe, the plasma system which used for the study is DC plasma from argon gas as well as Langmuir probe measurement. The construction hemisphere probe was connected to the network analyzer to measure the reflection coefficient and the match frequency. The experimental results which are the reflection coefficient, match frequency at any DC generated power are shown in Figure 45, and Figure 46.

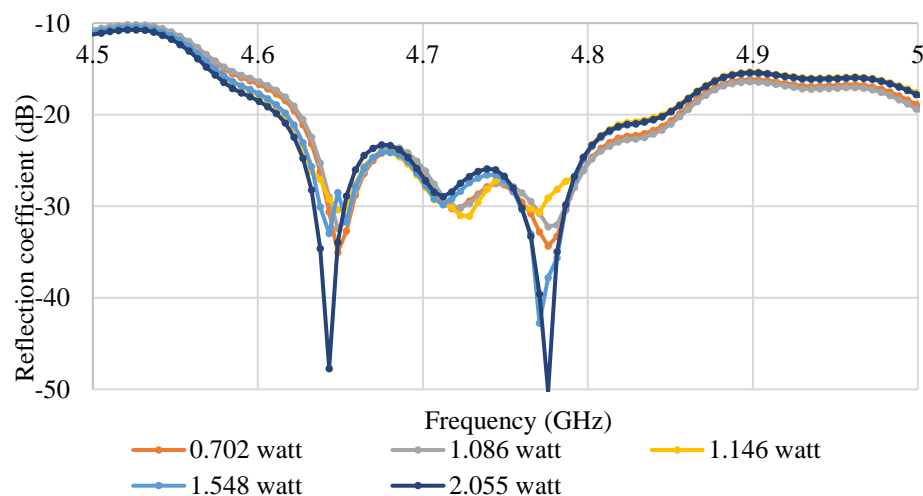


Figure 45 The reflection coefficients were obtained from the DC plasma by using the constructed hemisphere probe at any DC generated power

The match frequency can be collected from the minimum location of the reflection coefficient as shown in Figure 46.

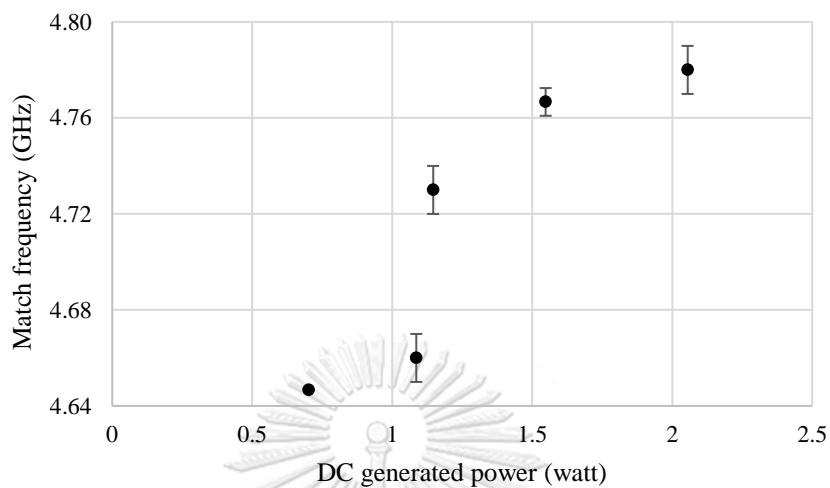


Figure 46 The match frequencies were obtained from the DC plasma by using the constructed hemisphere probe at any DC generated power

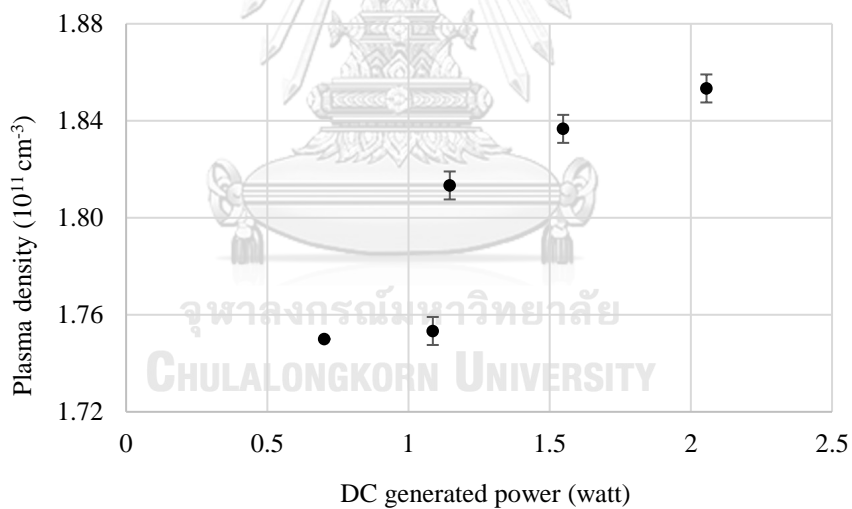


Figure 47 The plasma densities are obtained from the DC plasma by using the constructed hemisphere probe at any DC generated power

From the measurement of the plasma density by using the analytical solution of the constructed hemisphere probe in section 6.2, the result showed that the frequencies with the lowest reflection coefficient or match frequency of the experiment were in the range of 4.64 - 4.78 GHz. Based on the analytical solution of the hemisphere probe, the plasma frequency was considered by applying the result of the hemisphere match frequency by using simulation through MATLAB. Thus, the results of the plasma frequency can be directly used to find plasma density from the equation (72). The value of the plasma density from the experiment was in the range 1.74 - 1.85 ($\times 10^{11}$) cm^{-3} as shown in Figure 47.

According to Figures 45, 46, and 47, the results can be summarized in Table 3.

<i>DC generated power (watt)</i>	<i>Data set</i>	<i>Match frequency (GHz)</i>			<i>Plasma density (10^{11}cm^{-3})</i>		
		<i>Data</i>	<i>Average</i>	<i>Standard deviation</i>	<i>Data</i>	<i>Average</i>	<i>Standard deviation</i>
0.702	1	4.65			1.75		
	2	4.65	4.65	0.00	1.75	1.75	0.000
	3	4.65			1.75		
1.086	1	4.65			1.75		
	2	4.67	4.66	0.010	1.76	1.75	0.006
	3	4.66			1.75		
1.146	1	4.73			1.81		
	2	4.72	4.73	0.010	1.81	1.81	0.006
	3	4.74			1.82		
1.548	1	4.77			1.84		
	2	4.77	4.77	0.006	1.84	1.84	0.006
	3	4.76			1.83		
2.055	1	4.78			1.85		
	2	4.77	4.78	0.010	1.85	1.85	0.006
	3	4.79			1.86		

Table 3 Summary table of match frequency, and plasma densities from DC plasma measurement by using hemisphere probe

A comparison of the plasma density obtained from the analytical solution of the constructed hemisphere probe and the constructed Langmuir probe plasma density was shown in Figure 48.

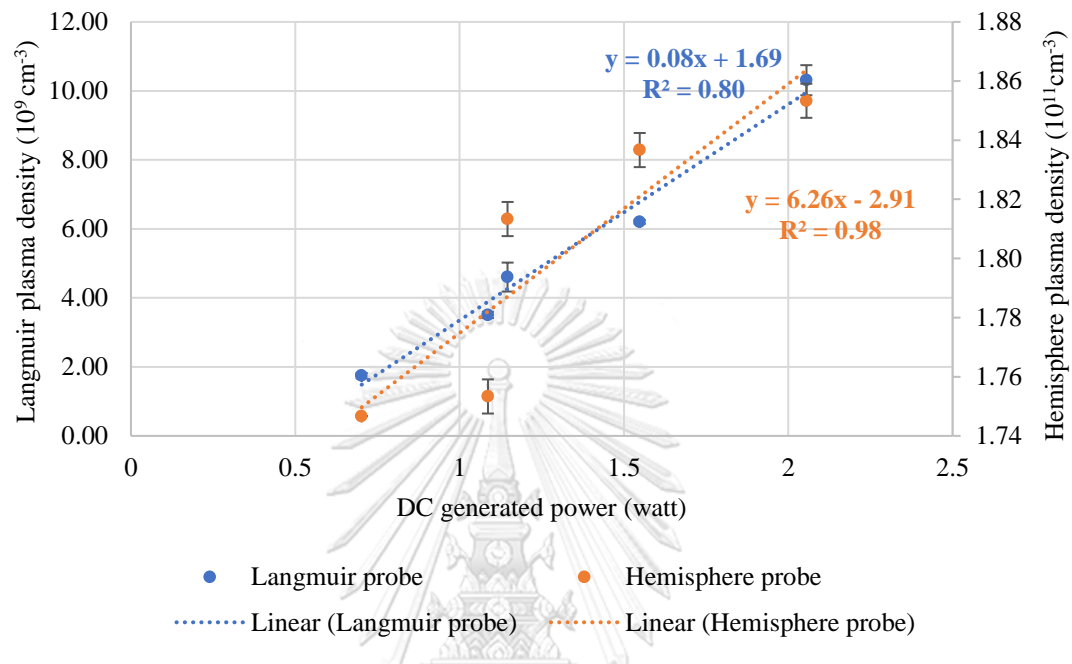


Figure 48 Comparison of the plasma density obtained from the constructed hemisphere probe and the constructed Langmuir probe

According to Figure 48, the results can be summarized as in Table 4.

DC generated power (watt)	Langmuir plasma density (10^9 cm^{-3})	Hemisphere plasma density (10^{11} cm^{-3})
0.702	1.75 ± 0.079	1.75 ± 0.000
1.086	3.51 ± 0.091	1.75 ± 0.006
1.146	4.60 ± 0.420	1.81 ± 0.006
1.548	6.20 ± 0.057	1.84 ± 0.006
2.055	10.31 ± 0.436	1.85 ± 0.006

Table 4 Summary table of plasma densities from DC plasma measurement by using Langmuir and hemisphere probe

According to Table 4, the constructed hemisphere probe and the conventional Langmuir probe responded with the change of the plasma parameters. The plasma density values of both methods increased when the DC plasma generated power increased. The plasma densities obtained from Langmuir are in order approximately 10^9 - 10^{10} and the plasma density from the hemisphere probe was in order approximately 10^{11} . Both values are approximately the second order of magnitude different.



7.2 MICROSTRIP PROBE MEASUREMENT

To study the plasma parameters by using the microstrip probe, the plasma system which used for the study is DC plasma from argon gas. Each length of the microstrip was connected with a network analyzer to obtain the reflection coefficient at various DC generated power. The reflection coefficient results are shown in Figure 49, and Figure 50.

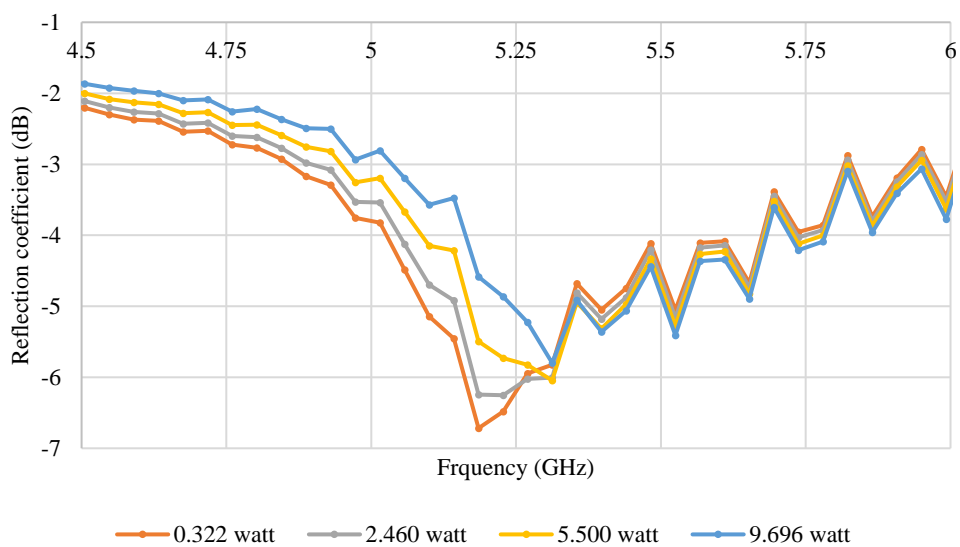


Figure 49 The reflection coefficient of the 16 mm. microstrip at any DC generated power

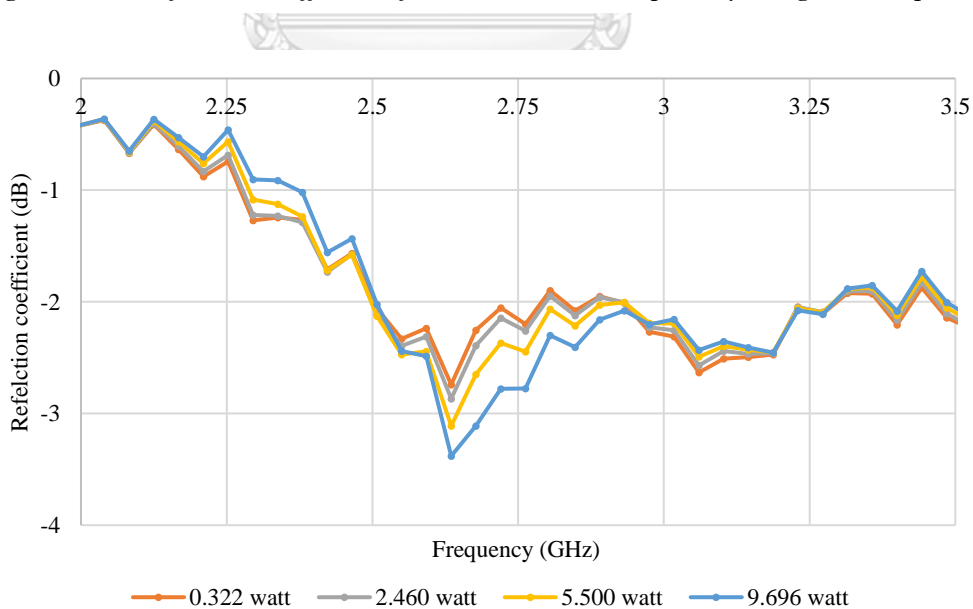


Figure 50 The reflection coefficient of the 21 mm. microstrip at any DC generated power

According to Figures 49 and 50, the results can be summarized as Table 5.

DC generated power (watt)	Data set	Match frequency (GHz)					
		16 mm. microstrip			21 mm. microstrip		
		Data	Average	Standard deviation	Data	Average	Standard deviation
0.702	1	5.19			2.65		
	2	5.19	5.19	0.000	2.65	2.65	0.000
	3	5.19			2.65		
1.086	1	5.2			2.65		
	2	5.19	5.20	0.010	2.66	2.65	0.006
	3	5.21			2.65		
1.146	1	5.21			2.66		
	2	5.21	5.21	0.006	2.66	2.66	0.006
	3	5.2			2.65		
1.548	1	5.21			2.66		
	2	5.22	5.22	0.006	2.67	2.66	0.006
	3	5.22			2.66		
2.055	1	5.23			2.67		
	2	5.25	5.24	0.012	2.68	2.68	0.006
	3	5.23			2.68		

Table 5 Summary table of the match frequency of 16 mm., and 21 mm. microstrip

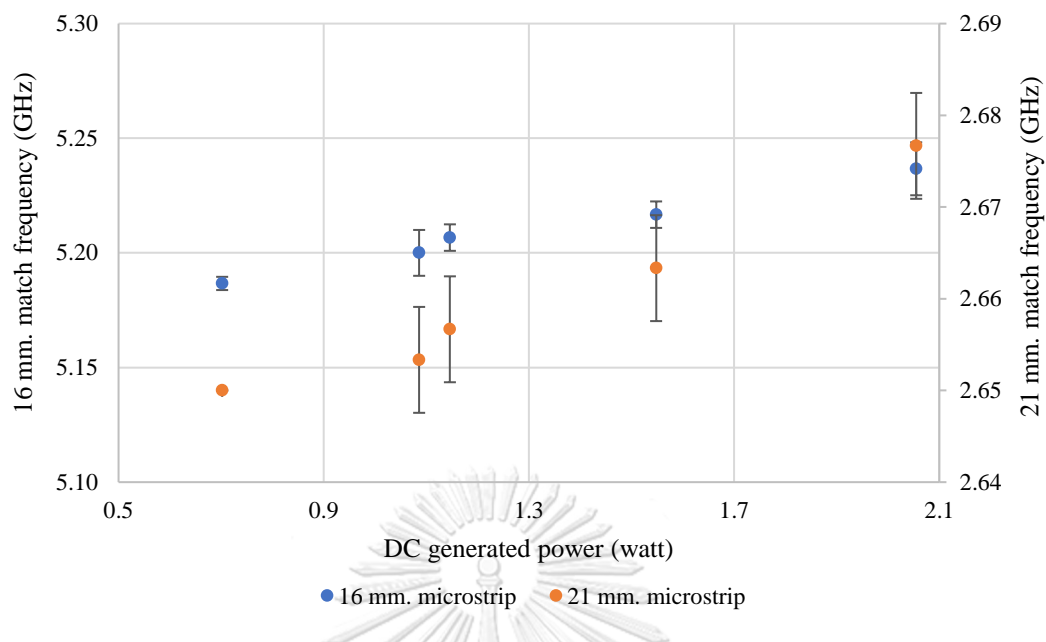


Figure 51 The plasma densities are obtained from the DC plasma by using the microstrip at any electric power

The experimental results of the reflection coefficient showed that the microstrip probe both with 16 mm. and 21 mm. responded with the change of plasma parameter. The match frequency values of both probes are different. It was shown that the match frequencies depended on the form of the probe tip.

7.3 PARALLEL PROBE MEASUREMENT

To study the plasma parameters by using the parallel probe, the plasma system which used for the study is DC plasma from argon gas as well as Langmuir probe measurement. Each length of the microstrip was connected with a network analyzer to obtain the reflection coefficient at various DC generated power. The reflection coefficient results are shown in Figure 52, and Figure 53.

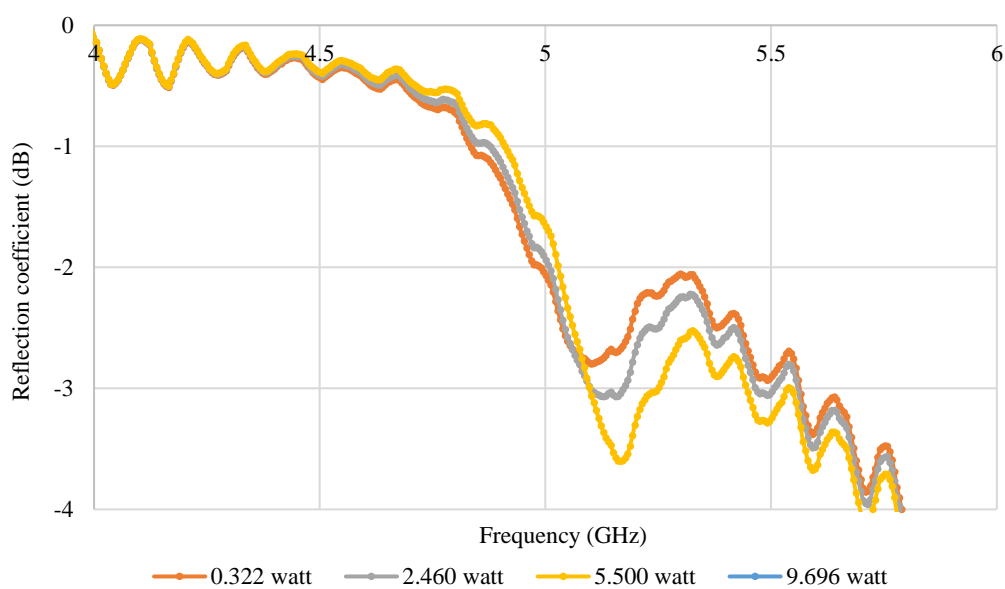


Figure 52 The reflection coefficient of the 16 mm. parallel at any DC generated power

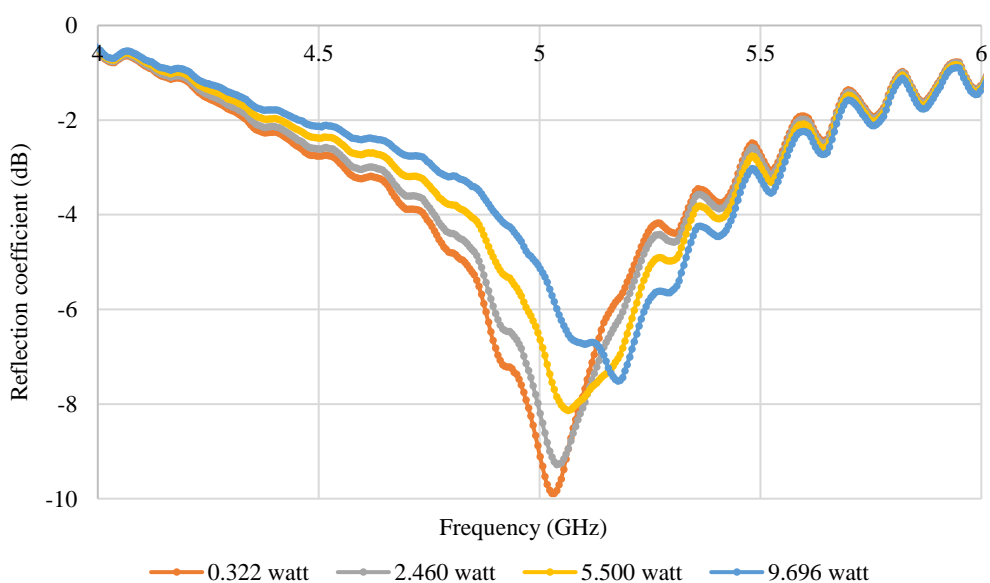


Figure 53 The reflection coefficient of the 21 mm. parallel at any DC generated power

According to Figures 52 and 53, the results can be summarized as Table 6.

DC generated power (watt)	Data set	Match frequency (GHz)					
		16 mm. parallel			21 mm. parallel		
		Data	Average	Standard deviation	Data	Average	Standard deviation
0.702	1	5.10			5.02		
	2	5.10	5.09	0.003	5.01	5.02	0.006
	3	5.09			5.02		
1.086	1	5.11			5.04		
	2	5.09	5.10	0.012	5.03	5.03	0.006
	3	5.11			5.03		
1.146	1	5.11			5.05		
	2	5.11	5.11	0.000	5.04	5.05	0.006
	3	5.11			5.05		
1.548	1	5.12			5.05		
	2	5.11	5.12	0.006	5.06	5.05	0.006
	3	5.12			5.05		
2.055	1	5.12			5.06		
	2	5.13	5.13	0.006	5.07	5.06	0.006
	3	5.13			5.06		

Table 6 Summary table of the match frequency of 16 mm., and 21 mm. parallel

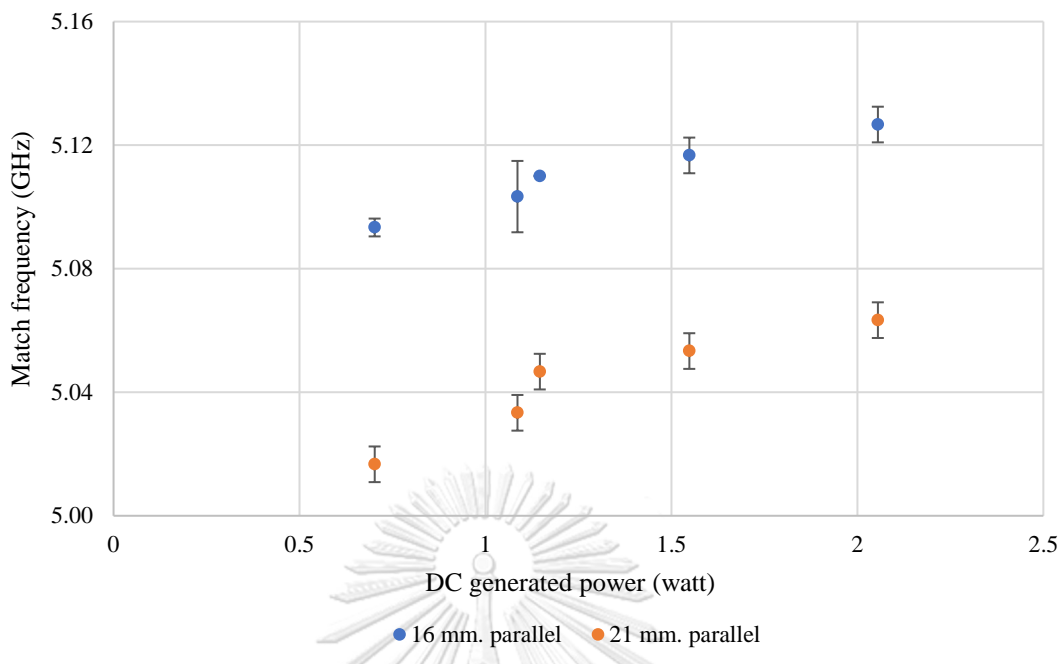


Figure 54 *The match frequencies are obtained from the DC plasma by using the microstrip at any DC generated power*

The experimental results of the reflection coefficient showed that the parallel probe both with 16 mm. and 21 mm. responded with the change of plasma parameter. The match frequency values of both are different. It was shown that the match frequencies depended on the length of the probe tip as in the case of the microstrip probe.

8. PROBE CALIBRATIONS

8.1 CHAPTER OVERVIEW

In order to find the plasma density of the APRS including hemisphere, microstrip, and parallel probe. It appeared that an analytical solution cannot be found. The simplest way is calibration by using the conventional Langmuir probe plasma density. The determination of the plasma density by using the Langmuir probe was used as a criterion because it is a method that has been widely used. The system's reflection coefficients over a range of frequencies are measured and analyzed into the match frequency. From equation (72), one could see that the plasma density is varied by the square of the frequency, therefore the calibration of plasma density obtained by Langmuir probe results to the square of MRP match frequency was performed.

In our calibration, the equation (72) which is obtained from the condition of resonance frequency must be changed because the probe was included as part of the transmission line. The impedance of the system was changed. Therefore, the plasma density results should be perturbed by such stray impedance of which, for simplification in the calculation, could be added as a geometrical factor. And due to the linear dependence nature of impedance to the frequency, a constant term can be added to equation (6) and becomes

$$n_e = n_{exp} + \Delta(\omega) \quad (100.1)$$

where

$$n_{exp} = (2\pi)^2 \frac{\epsilon_0 m_e \omega^2}{e^2} \quad (101.2)$$

n_{exp} is the experimental result of the plasma density

n_e is the result of the plasma density obtained from the Langmuir probe

$\Delta(\omega)$ is the geometrical factor

8.2 HEMISPHERE PROBE CALIBRATION

From the study of the reflection coefficient of the hemisphere probe. The results show that the match frequency responded with the change of DC generated power. Therefore, the hemisphere probe was calibrated by using the comparison of the hemisphere probe match frequencies square and the plasma density of the Langmuir probe. The results were shown in Figure 55.

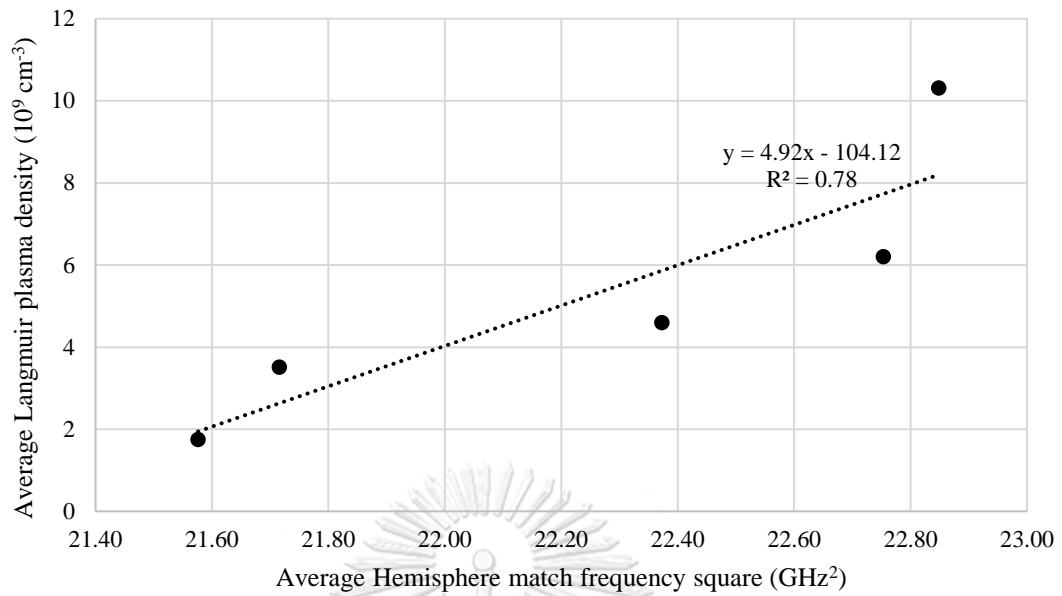


Figure 55 The relation of plasma density obtained from Langmuir probe and Hemisphere probe Match frequency

Consider Figure 55, the relation of the average plasma density obtained from the conventional Langmuir probe and the average hemisphere match frequency is

$$n_e = 4.92\omega^2 - 104.12 \quad (101)$$

According to Figure 55, the results can be summarized in Table 8.

DC generated Power (watt)	Average Langmuir plasma density (10 ⁹ cm ⁻³)	Average hemisphere probe match frequency (GHz)	Average hemisphere probe match frequency square (GHz ²)
0.702	1.75	4.65	21.58
1.086	3.51	4.66	21.72
1.146	4.60	4.73	22.37
1.548	6.20	4.77	22.75
2.055	10.31	4.78	22.85

Table 7 Summary table of plasma density from DC plasma measurement by using a Langmuir probe and hemisphere match frequency

8.3 MICROSTRIP PROBE CALIBRATION

From the study of the reflection coefficient of the microstrip probe. The results show that the match frequency responded with the change of DC generated power. Therefore, the microstrip probe was calibrated by using the comparison of the microstrip match frequencies square and the plasma density of the Langmuir probe. The results were shown in Figures 56 and 57.

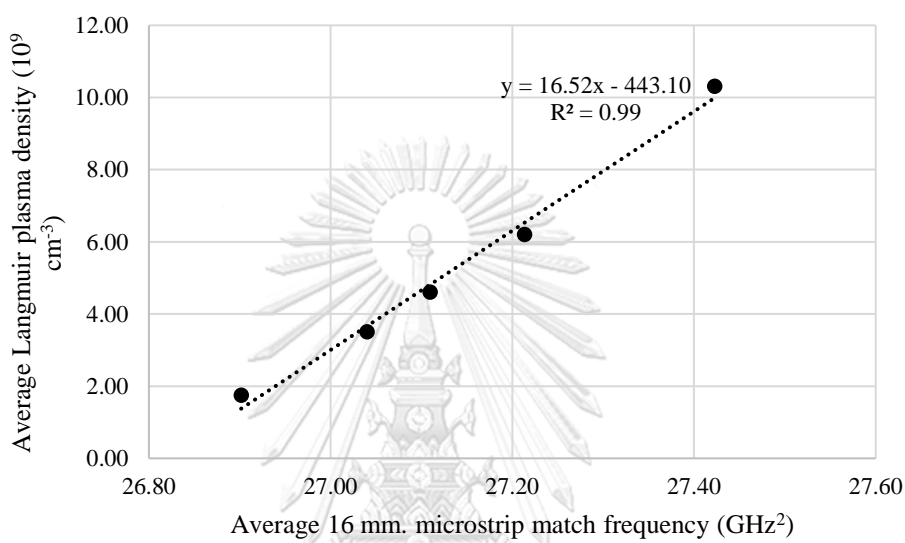


Figure 56 The relation of the average plasma density obtained from the Langmuir probe and the average 16 mm. microstrip match frequency square

Consider Figure 56, the relation of plasma density obtained from the conventional Langmuir probe and the 16 mm. microstrip match frequency square is

$$n_e = 16.52\omega^2 - 443.10 \quad (102)$$

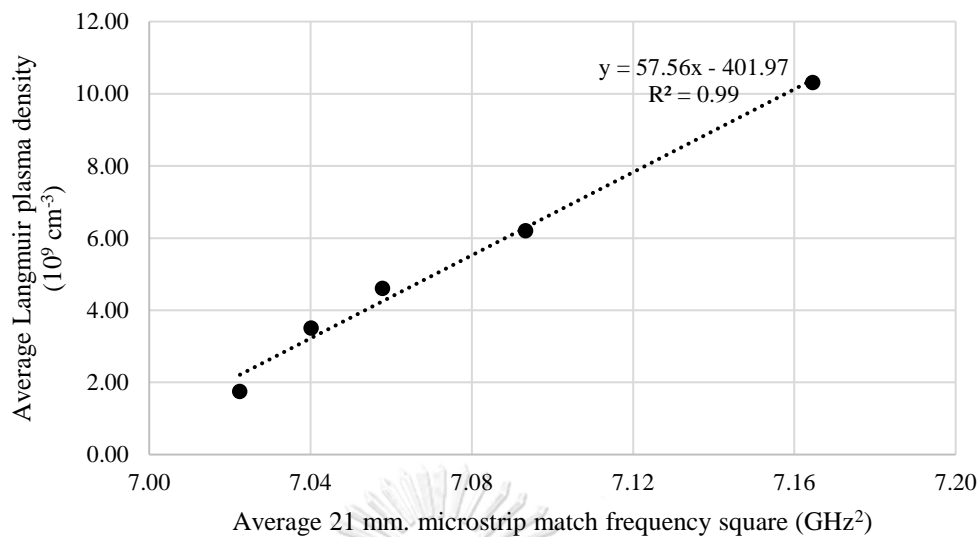


Figure 57 The relation of the average plasma density obtained from the Langmuir probe and the average 21 mm. microstrip match frequency square

Consider Figure 57, the relation of plasma density obtained from the conventional Langmuir probe and the 21 mm. microstrip match frequency square is

$$n_e = 57.56\omega^2 - 401.97 \quad (103)$$

According to Figure 56, and 57, the results can be summarized in Table 9.

DC generated power (watt)	Average Langmuir plasma density (10 ⁹ cm ⁻³)	Average microstrip match frequency (GHz)		Average microstrip match frequency square (GHz ²)	
		16 mm.	21 mm.	16 mm.	21 mm.
		0.702	1.75	5.19	2.65
1.086	3.51	5.20	2.65	27.04	7.04
1.146	4.60	5.21	2.66	27.11	7.06
1.548	6.20	5.21	2.66	27.21	7.09
2.055	10.31	5.23	2.67	27.42	7.16

Table 8 Summary table of plasma density from DC plasma measurement by using a Langmuir probe and Microstrip match frequency

8.4 PARALLEL PROBE CALIBRATION

From the study of the reflection coefficient of the parallel probe. The results show that the match frequency responded with the change of DC generated power. Therefore, the parallel probe was calibrated by using the comparison of the parallel match frequencies square and the plasma density of the Langmuir probe. The results were shown in Figures 58 and 59.

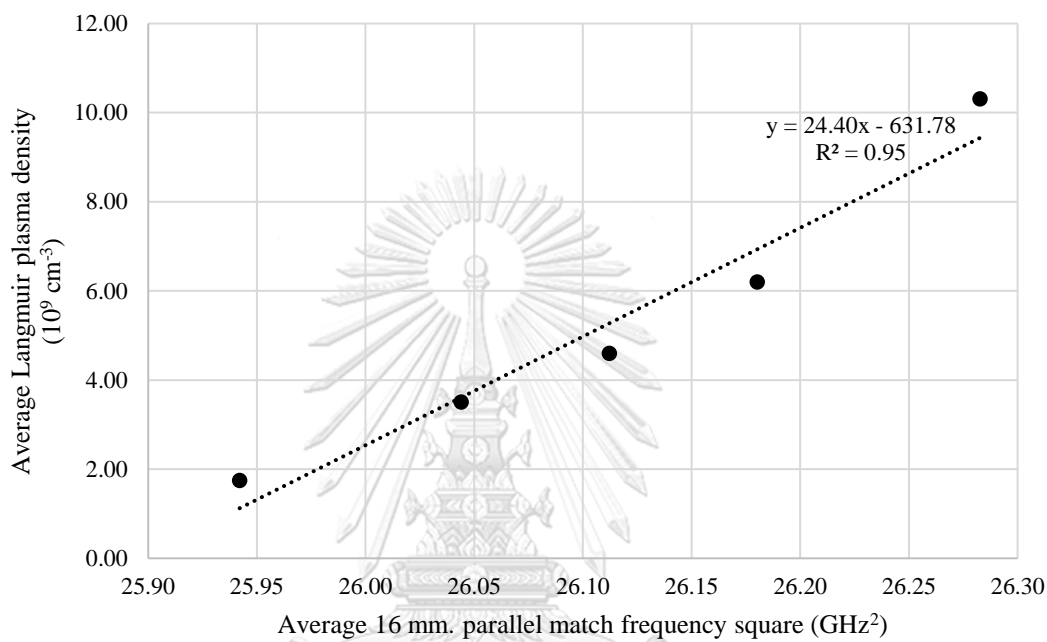


Figure 58 The relation of the average plasma density obtained from the Langmuir probe and the average 16 mm. parallel match frequency square

Consider Figure 58, the relation of plasma density obtained from the conventional Langmuir probe and the 16 mm. parallel match frequency square is

$$n_e = 24.40\omega^2 - 631.78 \quad (104)$$

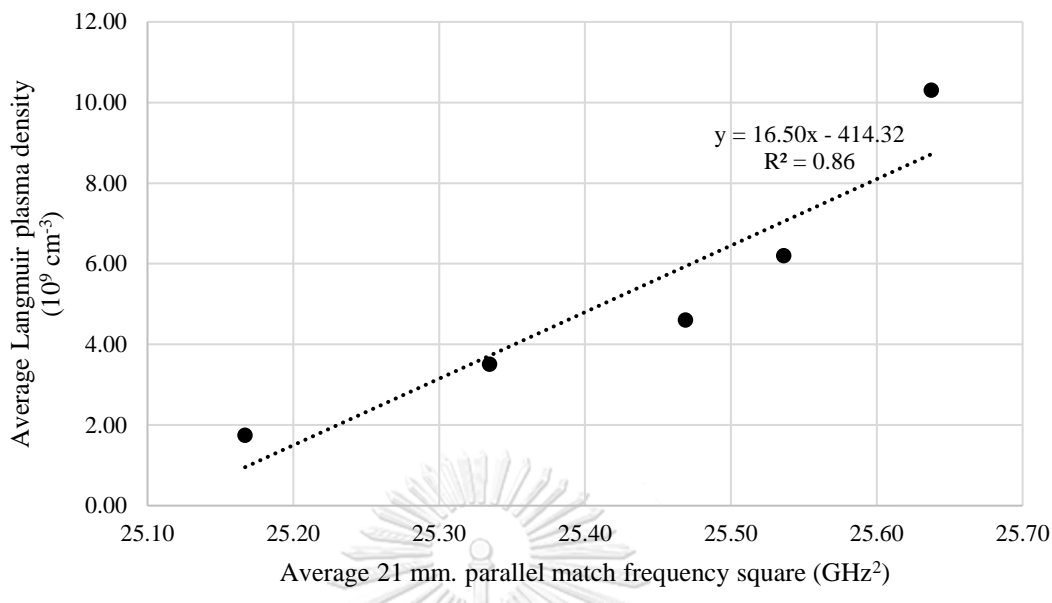


Figure 59 The relation of the average plasma density obtained from Langmuir probe and the average 21 mm. parallel match frequency square

Consider Figure 59, the relation of plasma density obtained from the conventional Langmuir probe and the 21 mm. parallel match frequency square is

$$n_e = 16.50\omega^2 - 414.32 \quad (105)$$

According to Figures 58, and 59, the results can be summarized in Table 10.

DC generated power (watt)	Average Langmuir plasma density (10 ⁹ cm ⁻³)	Average parallel match frequency (GHz)		Average parallel match frequency square (GHz ²)	
		16 mm.	21 mm.	16 mm.	21 mm.
		0.702	1.75	5.09	5.02
1.086	3.51	5.10	5.03	26.04	25.33
1.146	4.60	5.11	5.05	26.11	25.47
1.548	6.20	5.12	5.05	26.18	25.54
2.055	10.31	5.13	5.06	26.28	25.64

Table 9 Summary table of plasma density from DC plasma measurement by using a Langmuir probe and Microstrip match frequency

8.4 LANGMUIR PROBE PLASMA DENSITY AND MATCH FREQUENCY RELATION

From the calibration of APRS in each probe shapes which are hemisphere, microstrip, and parallel probe. We can summarize Figure 55 to Figure 59 into Figures 60 and 61 as follow

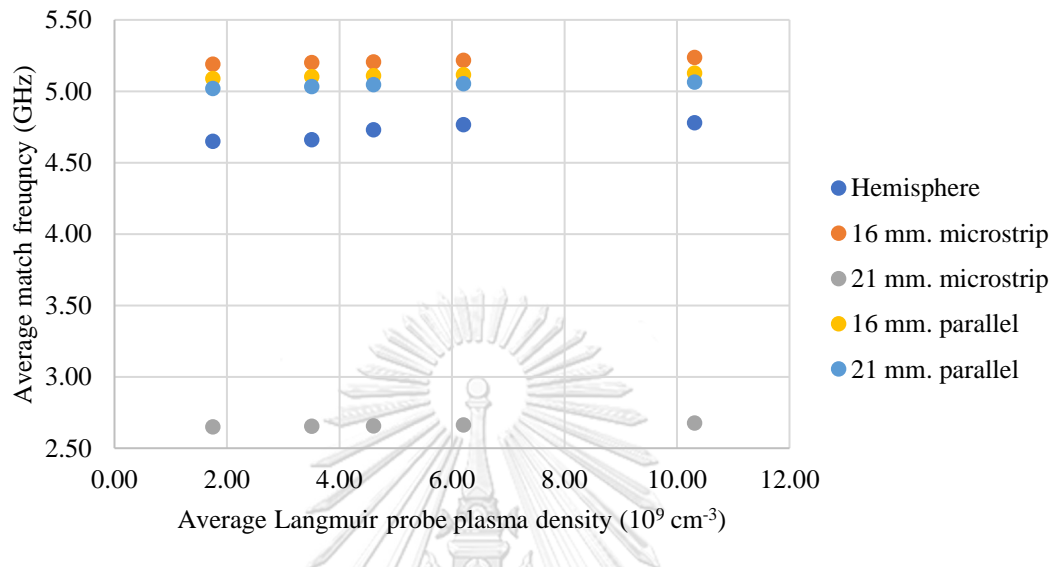


Figure 60 The relation between the average Langmuir probe plasma density and the match frequency of active resonance probe in each shape

According to Figure 60, the results can be summarized in Table 11.

Langmuir plasma density (10^9 cm^{-3})	Average match frequency (GHz)				
	Hemisphere probe	Microstrip probe		Parallel probe	
		16 mm.	21 mm.	16 mm.	21 mm.
1.75	4.65	5.19	2.65	5.09	5.02
3.51	4.66	5.20	2.65	5.10	5.03
4.60	4.73	5.21	2.66	5.11	5.05
6.20	4.77	5.22	2.66	5.12	5.05
10.31	4.78	5.24	2.68	5.13	5.06

Table 10 Summary table of the average plasma density from DC plasma measurement by using a Langmuir probe and the average match frequency of any probe shape

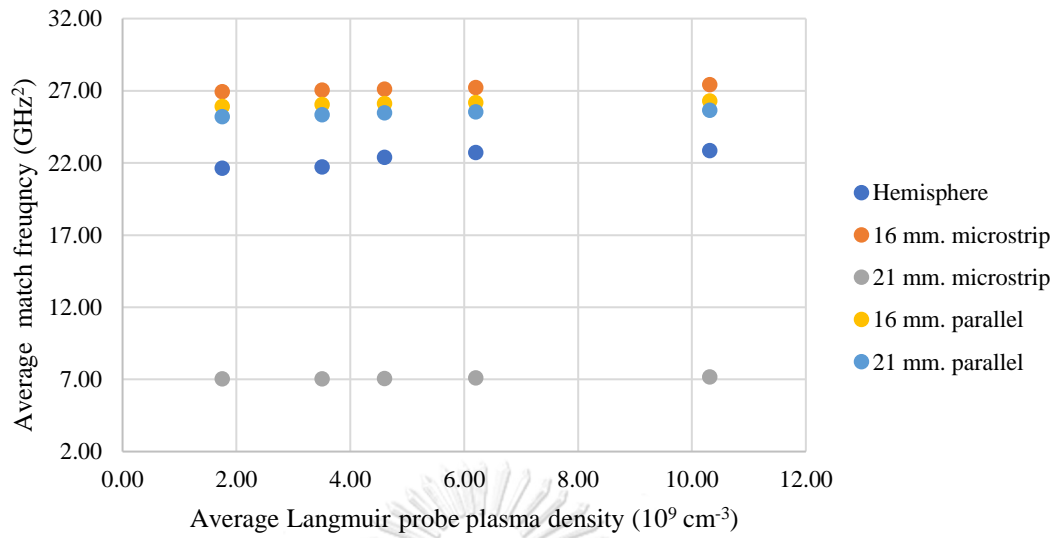


Figure 61 The relation between the average Langmuir probe plasma density and the average match frequency square of active resonance probe in each shape

According to Figure 61, the results can be summarized in Table 12.

Langmuir plasma density (10^9 cm^{-3})	Average match frequency square (GHz^2)				
	Hemisphere probe	Microstrip probe		Parallel probe	
		16 mm.	21 mm.	16 mm.	21 mm.
1.75	21.62	26.94	7.02	25.91	25.20
3.51	21.72	27.04	7.04	26.04	25.33
4.60	22.37	27.11	7.06	26.11	25.47
6.20	22.72	27.21	7.09	26.18	25.54
10.31	22.85	27.42	7.16	26.28	25.64

Table 11 Summary table of the average plasma density from DC plasma measurement by using a Langmuir probe and the average match frequency of any probe shape

9. DISCUSSION

In this research, we aimed to construct the active plasma resonance probe in different shapes which are hemisphere, microstrip, and parallel rod shapes. The constructed probe was used to measure the plasma density in the DC plasma discharge. The plasma density was also obtained by using Langmuir probe yielding which is the simple way to find the relation of the match frequency and the plasma density since the exact solution of the probes cannot be determined at the present, except for the hemisphere probe. The analytical solution of the hemisphere probe is known as a multipole resonance probe solution [7]. In our experiment, the analytical solution was used to find the plasma density.

The plasma density results obtained by the analytical solution of the hemisphere probe were compared with those of the Langmuir probe. The determination of the plasma density by using the Langmuir probe was used as a criterion because it is a method that has been widely accepted. The results show that the Langmuir probe and the hemisphere probes also respond well with the change with plasma generated power as shown in Figure 48. Unfortunately, there is some plasma density deviation in both experimental results. The value of the plasma density obtained from the mathematical solution is in the range of $1.74 - 1.85 (x10^{11}) \text{ cm}^{-3}$.

Recent work by Martin Lapke in 2011 [9], the multipole resonance probe was used to measure in a radio-frequency plasma discharge. The plasma density over generated power between 100 – 300 watts. The value of the plasma density is in the range of $0.20 - 1.00 (x10^{11}) \text{ cm}^{-3}$. To the best of the author's knowledge, there are no reports about using the multipole resonance probe measurement in DC plasma discharge.

In our experiment, there are several conditions that may cause deviation. From equation (72) which is obtained from the condition of resonance frequency in the transmission line. When the transmission line was added by the probes, the impedance of the system changed. Therefore, the plasma density results should be perturbed by such stray impedance of which, for simplification in the calculation, could be added as a geometrical factor. And due to the linear dependence nature of impedance to the frequency, a constant term can be added to equation (72) and becomes equation (100).

Secondly, the measurements were performed at high frequency. The impedance is very sensitive to the probe characteristic [19]. In our experiment, we consider an idealized case where the coaxial cable is neglected, and the hemisphere probe is considered as a perfect sphere. Consider the disturbance of the probe in plasma, the hemisphere probe disturbed the plasma much less than the Langmuir probe because the probe and plasma were considered as a system of electrical networks to measure match frequency instead of the biased voltages method used by Langmuir probe measurement.

As already stated, the plasma density deviation is somewhat pronounced, but it is interesting that the hemisphere can respond to DC generated power. From equation (72), one could see that the plasma density is varied by the square of the frequency, therefore the calibration of plasma density obtained by Langmuir probe results to the square of hemisphere match frequency was performed. The calibration result is shown in Figure 55. The linear fitting in Figure 55 to equation (100) yields the fitting result as in equation (101). The additional geometrical factor was found to be $-104.12 \times 10^9 \text{ cm}^{-3}$.

From the concept that the APRS probe can be of any shape [17], the experimental results of the reflection coefficient showed that the probes which are microstrip and parallel rod shapes also respond with the change in plasma similar to the hemisphere probe. When the DC generated power is increased, the match frequency is increased as well. Unfortunately, the plasma density cannot be directly obtained from the probes like a hemisphere probe since the exact solution of the probes cannot be determined analytically. Although the exact solution cannot be found, it can be seen that the results of the match frequency obtained from any shapes are different because the match frequency depends on the probe characteristics which affect the probe impedance. The probe impedance directly depends on the reflection coefficient spectrum and the match frequency location as shown in Figures 60 and 61.

Therefore, the calibration of plasma density obtained by the Langmuir probe results to the square of the probes match frequency could be performed to the same way as in hemisphere probe. The calibration result of the microstrip and parallel rods are shown in Figure 56 to Figure 59. The additional geometrical factor can be obtained as shown in equation (101) to (105).

10. SUMMARY

In this research, the active plasma resonance spectroscopy probe in the hemisphere, microstrip, and parallel rods shapes were successfully constructed and used to measure the match frequency and the reflection coefficient spectrum in DC plasma discharge. The results show that the probes also respond well with the change with plasma generated power. The plasma density can also be obtained by calibration against Langmuir probe. In this work, we can find the relation between the plasma density and the match frequency square due to the nature of the variable that the plasma density is varied by the square of the frequency as shown in equation (72). The linear fitting to find geometrical factors were performed.

For the hemisphere probe, the mathematical solution of the probe is known as a multipole resonance probe solution. The solution was used to find the plasma density and compared with the Langmuir probe measurement. The mathematical results have significantly deviated when compared with the conventional Langmuir probe. Our study showed that the plasma density from the mathematical model is approximately the second order of magnitude away from those of the Langmuir probe. There are several conditions that may cause deviation which are (i) The impedance of the system was changed by adding the probe because the equation (72) is obtained from the condition of resonance frequency in the transmission line. (ii) The impedance is very sensitive to the probe characteristic because we consider an idealized case where the coaxial cable is neglected, and the hemisphere probe is considered as a perfect sphere.

APPENDIX A

DEBYE LENGTH

Debye length occurs because of disturbing charges entering the plasma area. The plasma will be rearranged to prevent the potential increase. As the distance from the observation point to the disturbance charge increases. It is obvious that the disturbance potential is greatly reduced. Therefore, it can be concluded that the area beyond the Debye length is an undisturbed plasma. The Debye length can be proven from the Poisson equation due to the difference in ion and electron density at the plasma sheath area as follows

$$\nabla^2 \Phi = -\frac{e}{\epsilon_0} [(n_i - n_e) + \delta(\vec{r})] \quad (106)$$

where n_i is the density of ions
 n_e is the density of electrons
 $\delta(\vec{r})$ is the Dirac delta function of the disturbance charge
 Φ is an electric potential

From the Boltzmann relation, equation (10) describes the density of the electrons and the neutral properties of the plasma.

$$\nabla^2 \Phi = \frac{en}{\epsilon_0} \left(\exp \frac{e\Phi(\vec{r})}{kT_e} - 1 \right) + \frac{e}{\epsilon_0} \delta(\vec{r}) \quad (107)$$

where the electric potential is much lower than the electron temperature, the relation (107) can distribute the power series as follows

$$\nabla^2 \Phi = \left(\frac{ne^2}{kT_e \epsilon_0} \right) \Phi + \frac{e}{\epsilon_0} \delta(\vec{r}) \quad (108)$$

Relations (108) can be rewritten as follows

$$\nabla^2 \Phi - \frac{1}{\lambda_D^2} = \frac{e}{\epsilon_0} \delta(\vec{r}) \quad (109.1)$$

$$\lambda_D = \sqrt{\frac{kT_e \epsilon_0}{ne^2}} \quad (109.2)$$

where λ_D is Debye length

The solution of the relation (109.1) can find as follows

$$\Phi(\vec{r}) = \frac{e}{4\pi\epsilon_0 r} \exp\left(-\frac{r}{\lambda_D}\right) \quad (110)$$

PLASMA FREQUENCY

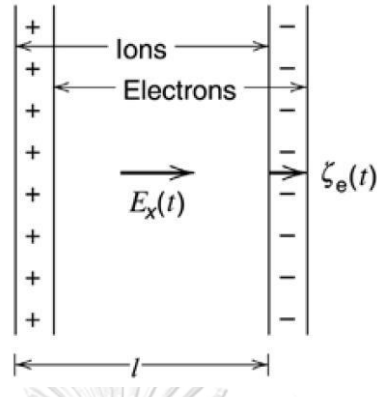


Figure 62 The occurrence of an electric field when the electron particles move in 2D[1]

Consider plasma in 2 dimensions. When electrons are moving. The ions induce an electric field E_x in the x-axis. The forces that can be considered for electrons particles [1] are as follows:

$$m_e \frac{d^2 \xi_e}{dt^2} = -eE_x \quad (111)$$

$$E_x = \frac{en_0 \xi_e}{\epsilon_0} \quad (112)$$

where m_e is the electron mass

ξ_e is a small distance that the electrons are moving

Substitute (112) into (111), the equation can be written as follows

$$\frac{d^2 \xi_e}{dt^2} = -\omega_{pe}^2 \xi_e \quad (113.1)$$

where

$$\omega_{pe} = \left(\frac{e^2 n_0}{\epsilon_0 m_e} \right)^{\frac{1}{2}} \quad (113.2)$$

MAXWELL VELOCITY DISTRIBUTION

Velocity is a vector quantity which can be written in the form of cartesian coordinates in the x, y, and z-axis as follows:

$$f(\vec{v}) = f(v_x, v_y, v_z) \quad (114)$$

$$f(\vec{v}) = n_e \left(\frac{m_e}{2\pi k T_e} \right)^{\frac{3}{2}} \exp \left(- \frac{m_e (v_x^2 + v_y^2 + v_z^2)}{2k T_e} \right) \quad (115)$$

Changing variables from the cartesian coordinates to the spherical coordinates by using the reference axis in Figure 63 with the equation (115)

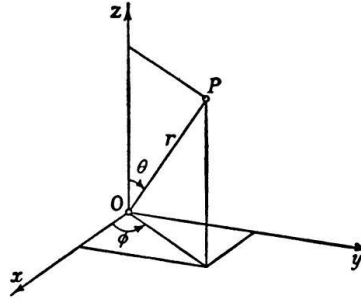


Figure 63 Reference axis for the cartesian coordinates to the spherical coordinates in 3D [1]

$$v_x = v_r \sin v_\theta \cos v_\phi \quad (116.1)$$

$$v_y = v_r \sin v_\theta \sin v_\phi \quad (116.2)$$

$$v_z = v_r \cos v_\theta \quad (116.3)$$

$$f(v_r) = f(v_x, v_y, v_z) = n_e \left(\frac{m_e}{2\pi k T_e} \right)^{\frac{3}{2}} 4\pi v^2 \exp \left(- \frac{m_e v_r^2}{2k T_e} \right) \quad (117)$$

where v_r is the magnitude of the velocity

Calculation of the average speed $\langle v \rangle$

$$\langle v \rangle = \frac{\int_0^\infty v_r f(v_r) dv_r}{n_e} \quad (118.1)$$

$$= \sqrt{\frac{8kT_e}{\pi m_e}} \quad (118.2)$$

Calculation of the electron flux in one dimension Γ

$$\Gamma = \int_0^{2\pi} \int_0^{\pi/2} \int_0^\infty v_r \cos v_\theta f(v_r, v_\theta, v_\phi) v_r^2 \sin v_\theta dv_r dv_\theta dv_\phi \quad (119.1)$$

$$= \frac{1}{4} \int_0^{2\pi} \int_0^{\pi/2} \int_0^\infty v_r f(v_r, v_\theta, v_\phi) v_r^2 \sin 2v_\theta dv_r d2v_\theta dv_\phi$$

$$\Gamma = \frac{1}{4} \int_0^\infty f(v_r) dv_r = \frac{1}{4} n_e \langle v \rangle \quad (119.2)$$

BOLTZMANN RELATION

When the electrons are inside the thermal equilibrium. Therefore, electrons do not have drift velocity. It can be concluded that the electrons are balanced between the electrical force and the gradient of pressure as follows

$$en_e\vec{E} + \vec{\nabla}p_e = 0 \quad (120)$$

where p_e is the electron pressure
 n_e is the electron density
 e is the electron charge

The electric field within the plasma can be explained by electrostatic theory and the behavior of electrons in gas theory as follows

$$\vec{E} = -\vec{\nabla}\Phi \quad (121)$$

$$p_e = n_e kT_e \quad (122)$$

Substitute the equation (121) and (122) into the equation (120) and reformat

$$-en_e\vec{\nabla}\Phi + kT_e\vec{\nabla}n_e = 0 \quad (123)$$

$$\vec{\nabla}(e\Phi - kT_e \ln n_e) = 0 \quad (124)$$

Found that the value $e\Phi - kT_e \ln n_e$ is a constant. It can be written as a new equation as follows

$$n_e(\vec{r}) = n_0 \exp\left(\frac{e\Phi(\vec{r})}{kT_e}\right) \quad (125)$$

SHEATH EQUATION

The sheath equation without particle collisions [11] can be considered by the Poisson equation due to the difference in ion and electron density at the plasma sheath.

$$\frac{d^2\Phi}{dx^2} = \frac{e}{\epsilon_0}(n_e - n_i) \quad (126)$$

Finding the density of ions, the energy conservation equation of ion without collisions, and the continuity equation of the ion flux

$$\frac{1}{2}Mu(x)^2 = \frac{1}{2}Mu_s^2 - e\Phi(x) \quad (127)$$

$$n_i(x)u(x) = n_{is}u_s \quad (128)$$

where

- M is ion mass
- n_i is the ion density
- n_{is} is ion density at the plasma sheath area
- n_{es} is electron density at the plasma sheath area
- u_s is the speed of positive charges before entering the sheath
- $u(x)$ is the velocity of the positive charge at the distance x from the sheath

From the equation (125), substituting $u(x)$ in the equation (127)

$$n_i = n_{is} \left(1 - \frac{2e\Phi}{Mu_s^2}\right)^{\frac{1}{2}} \quad (129)$$

the equation (129) is the ion density that is unknown at first. The density of electrons can be obtained from the Boltzmann relation (125).

$$n_e = n_{es} \exp\left(\frac{e\Phi}{kT_e}\right) \quad (130)$$

Assign $n_{is} = n_{es} = n_s$ and substitute (125) and (130) into Poisson's equation (126) to get a sheath equation without particle collision (11.1).

$$\frac{d^2\Phi(x)}{dx^2} = \frac{en_s}{\epsilon_0} \left[\exp\left(\frac{e\Phi(x)}{kT_e}\right) - \left(1 - \frac{\Phi(x)}{\epsilon_s}\right)^{\frac{1}{2}} \right] \quad (131)$$

APPENDIX B

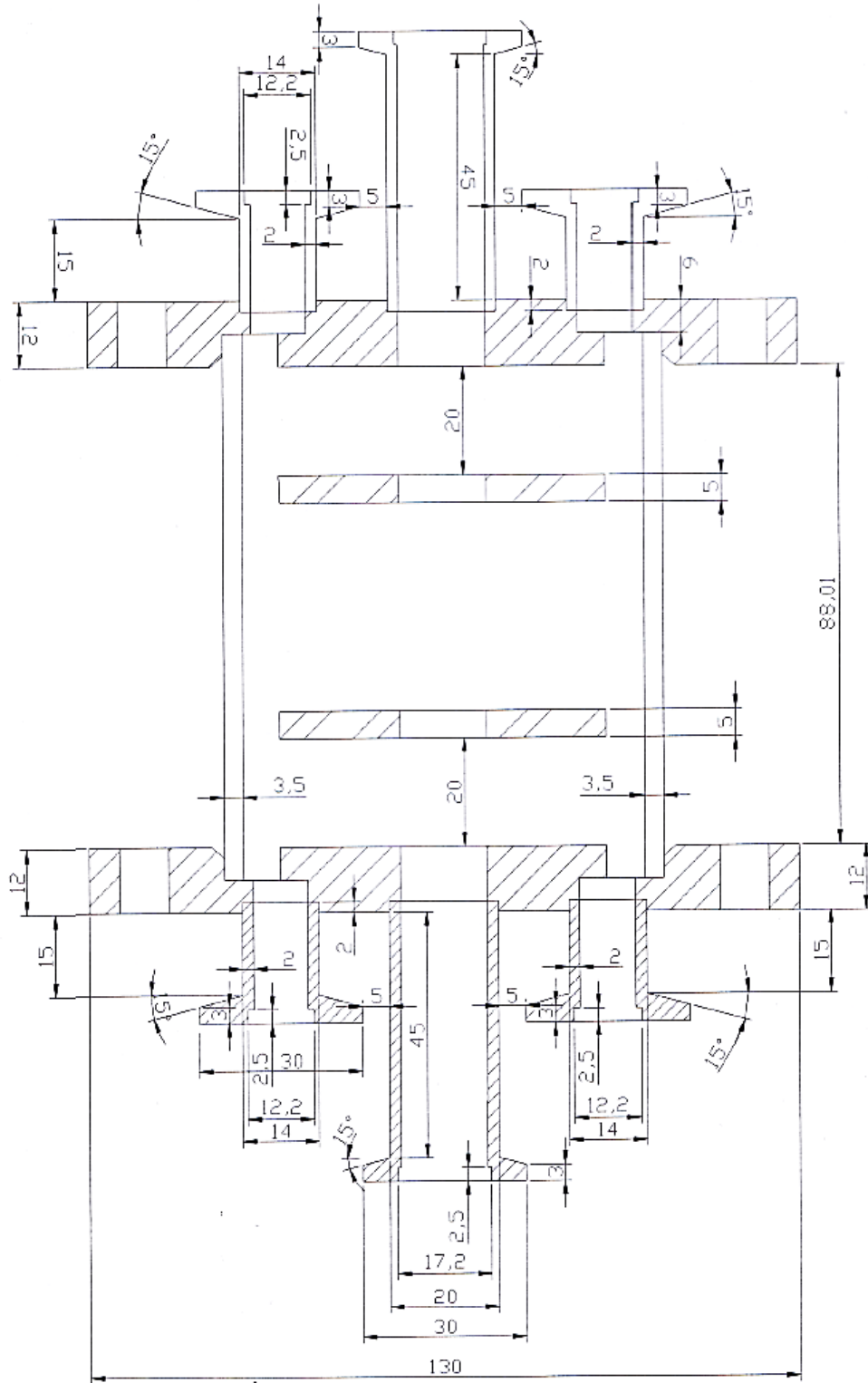


Figure 64 Vacuum container flange

REFERENCES

1. Chen FF. Plasma Physics. 2nd ed: Springer; 2006.
2. Schulz C, Styrnoll T, Awakowicz P, Rolfes I. The Planar Multipole Resonance Probe: Challenges and Prospects of a Planar Plasma Sensor. IEEE Transactions on Instrumentation and Measurement. 2014.
3. Shirakawa T, Sugai H. Plasma oscillation method for measurements of absolute electron density in plasma. Japanese Journal of Applied Physics. 1993;32(11 R):5129-35.
4. Stenzel RL. Microwave resonator probe for localized density measurements in weakly magnetized plasmas. Review of Scientific Instruments. 1976;47(5):603-7.
5. Kokura H, Nakamura K, Ghanashev IP, Sugai H. Plasma Absorption Probe for Measuring Electron Density in an Environment Soiled with Processing Plasmas. Japanese Journal of Applied Physics, Part 1: Regular Papers and Short Notes and Review Papers. 1999;38(9 A):5262-6.
6. Lapke M, Oberrath J, Mussenbrock T, Brinkmann RP. Active plasma resonance spectroscopy: A functional analytic description. Plasma Sources Science and Technology. 2013;22(2).
7. Lapke M, Mussenbrock T, Brinkmann RP. The multipole resonance probe: A concept for simultaneous determination of plasma density, electron temperature, and collision rate in low-pressure plasmas. Applied Physics Letters. 2008;93(5).
8. Piejak RB, Godyak VA, Garner R, Alexandrovich BM, Sternberg N. The hairpin resonator: A plasma density measuring technique revisited. Journal of Applied Physics. 2004;95(7):3785-91.
9. Lapke M, Oberrath J, Schulz C, Storch R, Styrnoll T, Zietz C, et al. The multipole resonance probe: Characterization of a prototype. Plasma Sources Science and Technology. 2011;20(4).
10. Meshcheryakova E, Zibrov M, Kaziev A, Khodachenko G, Pisarev A. Langmuir Probe Diagnostics of Low-pressure Inductively Coupled Argon Plasmas in a Magnetic Field. Physics Procedia. 2015;71:121-6.
11. Lieberman MA, Lichtenberg AJ. Principle of Plasma Discharges and Materials Processing: John Wiley & Sons; 2005.
12. Mott-Smith HM, Langmuir I. The theory of collectors in gaseous discharges. Physical

Review. 1926;28(4):727-63.

13. Lapke M, Mussenbrock T, Brinkmann RP, Scharwitz C, Böke M, Winter J. Modeling and simulation of the plasma absorption probe. *Applied Physics Letters*. 2007;90(12).
14. Friedrichs M, Oberrath J. The planar Multipole Resonance Probe: a functional analytic approach. *EPJ Techniques and Instrumentation*. 2018;5(1):7.
15. Liang I, Nakamura K, Sugai H. Modeling microwave resonance of curling probe for density measurements in reactive plasmas. *Applied Physics Express*. 2011;4(6).
16. Scharwitz C, Böke M, Winter J, Lapke M, Mussenbrock T, Brinkmann RP. Practical implementation of a two-hemisphere plasma absorption probe. *Applied Physics Letters*. 2009;94(1).
17. Oberrath J, Brinkmann RP. Active plasma resonance spectroscopy: Eigenfunction solutions in spherical geometry. *Plasma Sources Science and Technology*. 2014;23(6).
18. Staack D, Farouk B, Gutsol A, Fridman A. Characterization of a dc atmospheric pressure normal glow discharge. *Plasma Sources Science and Technology*. 2005;14(4):700-11.
19. Pozar DM. *Microwave Engineering*. 4th ed: John Wiley & Sons; 1998.
20. Jackson JD. *Classical Electrodynamics*. 1st ed: John Wiley & Sons; 1962.
21. Arfken GB, Weber HJ, Harris FE. *Mathematical Methods for Physicists*. 7th ed: Academic Press; 2012.
22. Riley KF, Hobson MP, Bence SJ. *Mathematical Methods for Physics and Engineering : A Comprehensive Guide*. 3rd Revised edition ed: CAMBRIDGE UNIVERSITY PRESS; 2006.
23. Griffiths DJ. *Introduction to Electrodynamics*. 4th edition ed: Pearson Cambridge University Press; 1999.



จุฬาลงกรณ์มหาวิทยาลัย
CHULALONGKORN UNIVERSITY

VITA

NAME Natthapong Jampaiboon
DATE OF BIRTH 18 October 1995
PLACE OF BIRTH Chachoengsao, Thailand
INSTITUTIONS ATTENDED Chulalongkorn University
HOME ADDRESS 51/6 Moo 15, Takai, Muang, Chachoengsao, 24000

